Article

Neuron

# Dysregulation of Prefrontal Cortex-Mediated Slow-Evolving Limbic Dynamics Drives Stress-Induced Emotional Pathology

## Highlights

- Prefrontal cortex (PFC) oscillations synchronize with ultraslow limbic dynamics
- PFC unit firing signals the synchronization state of amygdala (AMY) and ventral tegmental area (VTA)
- Chronic stress selectively disrupts PFC-dependent regulation of AMY-VTA synchrony
- PFC to AMY circuit stimulation recovers normal network function and behavior

## Authors

Rainbo Hultman, Stephen D. Mague, Qiang Li, ..., Karl Deisseroth, Scott D. Moore, Kafui Dzirasa

## Correspondence

kafui.dzirasa@duke.edu

## In Brief

The complex mechanisms whereby multiple brain regions coordinate emotion remain tenebrous. Hultman et al. show that the prefrontal cortex (PFC) directly regulates beta oscillatory connectivity between multiple limbic brain regions. Stress-induced disruption of this PFC-dependent function yields pathological emotional behavior.

Hultman et al., 2016, Neuron *91*, 439–452
July 20, 2016 
http://dx.doi.org/10.1016/j.neuron.2016.05.038

CellPress

Neuron
Article

# Dysregulation of Prefrontal Cortex-Mediated Slow-Evolving Limbic Dynamics Drives Stress-Induced Emotional Pathology

Rainbo Hultman,[1] Stephen D. Mague,[1] Qiang Li,[1] Brittany M. Katz,[1] Nadine Michel,[1] Lizhen Lin,[7] Joyce Wang,[1] Lisa K. David,[1] Cameron Blount,[1] Rithi Chandy,[1] David Carlson,[6] Kyle Ulrich,[6] Lawrence Carin,[6] David Dunson,[5] Sunil Kumar,[1] Karl Deisseroth,[8] Scott D. Moore,[1] and Kafui Dzirasa[1,2,3,4,*]
[1]Department of Psychiatry and Behavioral Sciences
[2]Center for Neuroengineering
[3]Duke Institute for Brain Sciences
Duke University Medical Center, Durham, NC 27710, USA
[4]Departments of Biomedical Engineering and Neurobiology
[5]Department of Statistical Sciences
[6]Department of Electrical and Computer Engineering
Duke University, Durham, NC 22208, USA
[7]Department of Statistics and Data Science, University of Texas at Austin, Austin, TX 78712, USA
[8]Departments of Bioengineering and Psychiatry and Howard Hughes Medical Institute, Stanford University, Stanford, CA 94305, USA
*Correspondence: kafui.dzirasa@duke.edu
http://dx.doi.org/10.1016/j.neuron.2016.05.038

## SUMMARY

**Circuits distributed across cortico-limbic brain regions compose the networks that mediate emotional behavior. The prefrontal cortex (PFC) regulates ultra-slow (<1 Hz) dynamics across these networks, and PFC dysfunction is implicated in stress-related illnesses including major depressive disorder (MDD). To uncover the mechanism whereby stress-induced changes in PFC circuitry alter emotional networks to yield pathology, we used a multi-disciplinary approach including in vivo recordings in mice and chronic social defeat stress. Our network model, inferred using machine learning, linked stress-induced behavioral pathology to the capacity of PFC to synchronize amygdala and VTA activity. Direct stimulation of PFC-amygdala circuitry with DREADDs normalized PFC-dependent limbic synchrony in stress-susceptible animals and restored normal behavior. In addition to providing insights into MDD mechanisms, our findings demonstrate an interdisciplinary approach that can be used to identify the large-scale network changes that underlie complex emotional pathologies and the specific network nodes that can be used to develop targeted interventions.**

## INTRODUCTION

Major depressive disorder (MDD) is a multifactorial mental disorder characterized by changes in mood, interests, sleep, and perception. While many genes and cells have been implicated in the onset and manifestation of depression, a concerted mechanism of causality has remained elusive, in part due to the heterogeneity of the disorder. Multiple human imaging studies have implicated altered functional activation of the prefrontal cortex (PFC) in MDD (Mayberg et al., 1999). Hyper-connectivity (i.e., increased oscillatory synchrony) between PFC and the default mode network has been directly linked to the duration of depressive episodes (Greicius et al., 2007), and an increase in the functional connectivity between PFC and both cognitive and limbic affective networks has been described in depressed subjects as well (Sheline et al., 2010). Finally, direct stimulation of sub-regions of the PFC ameliorates MDD symptoms and related behaviors in select clinical populations (George et al., 2010; Mayberg et al., 2005) and in multiple preclinical models of the disorder (Covington et al., 2010; Kumar et al., 2013). These findings suggest that dysfunction within PFC-dependent networks may serve as a pathophysiological mechanism underlying MDD. Here, we employ a novel interdisciplinary approach to test this hypothesis. Our goal was to test whether functional changes in PFC-dependent networks directly contribute to (rather than simply reflect) the global changes in limbic oscillatory connectivity and the behavioral alterations that occur with the disorder.

In humans, MDD can be triggered, exacerbated, or re-occur in response to stress (Bartolomucci and Leopardi, 2009; Caspi et al., 2003; Kendler et al., 1999; Tennant, 2002). Similarly, in rodents, exposure to chronic social defeat stress induces a syndrome that recapitulates many phenotypes of MDD (Golden et al., 2011; Krishnan et al., 2007). In this paradigm, animals are repeatedly exposed to larger aggressive animals for 10–15 consecutive days. At the end of this protocol, animals exhibit multiple depressive endophenotypes including hedonic dysfunction, circadian dysregulation, anxiety, and psychomotor retardation during the forced swim test (Krishnan et al., 2007; Warren et al., 2013). Furthermore, phenotypic responses to the

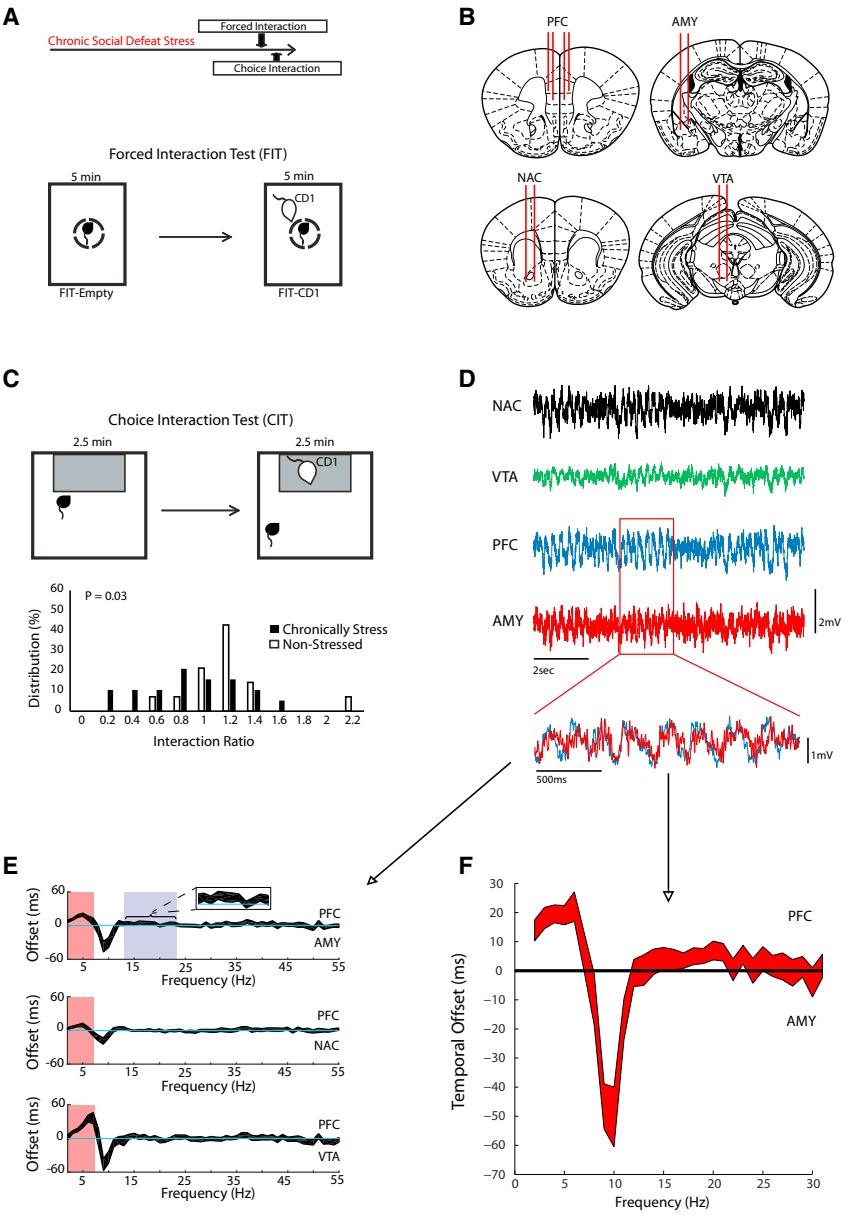


**Figure 1. PFC-Directed Oscillatory Interactions**

(A) Schematic of experimental timeline (top) and the FIT (bottom).

(B) Electrophysiological recording sites.

(C) Schematic of classic choice social interaction test (top), and interaction ratio scores measured in stressed mice and non-stressed controls (bottom; p = 0.03 using rank-sum test).

(D) Representative LFP traces. In the overlaid traces below, note that PFC oscillations (blue) tended to precede AMY oscillations (red).

(E) Using LFP data obtained during the second half of the forced interaction, we quantified the extent to which PFC phase synchronized with activity in the limbic regions. We then introduced step-wise temporal shifts between PFC oscillations and the other LFPs. Finally, we re-calculated the phase synchrony between these two regions and extracted the directionality based on the optimal time offset at which each brain region synchronized with PFC for each frequency. Data are shown as the 95% confidence intervals (N = 33 mice). PFC activity preceded all three of the other regions in 2–7 Hz band (red highlight), and AMY activity in the 14–23 Hz band.

(F) To confirm that PFC and AMY exhibited directionality in the beta frequency range (14–23 Hz), we calculated LFP phase coherence at various temporal offsets in a second cohort of animals implanted with wires in PFC and AMY (N = 46 mice; data show 95% confidence interval).

paradigm are sensitive to multiple distinct treatments that ameliorate symptoms in MDD and bipolar depression in humans. These treatments include cortical brain stimulation (Covington et al., 2010; Kumar et al., 2013), tricyclic antidepressants (Berton et al., 2006), selective serotonin reuptake inhibitors (Berton et al., 2006), ketamine (Donahue et al., 2014), and anticonvulsants (Berton et al., 2006). Now, we have clarified the role of PFC-dependent circuitry in mediating MDD-related behavioral and network phenotypes using the rodent model.

To directly probe the relationship between PFC circuitry, limbic network oscillatory dysfunction, and the emergence of depression-related behavior, we used the following systematic approach. First, we implanted mice with microwire recording electrodes in PFC and three relevant limbic brain regions implicated in MDD: nucleus accumbens (NAc), amygdala (AMY), and ventral tegmental area (VTA). We subjected the mice to chronic social defeat stress and recorded local field potential (LFP) oscillations and PFC unit activity. We identified all of the oscillatory frequencies at which the PFC influenced neural activity in the other limbic regions, and these oscillatory signals were selected as the input parameters for our neural network model of depression. Next, we used a translational depression-related assay, the forced interaction test (FIT), which involves exposure to an acute stressor. We measured the impact of this stressor on the oscillatory input parameters (Figure 1; see also Figure S1, available online) and then inferred a network model of depression that describes the relationship between the observed behavior and circuit physiology using supervised machine learning. Finally, we validated the "depression" network by directly stimulating a key node at the intersection of PFC and AMY circuitry in chronically stressed susceptible mice. Importantly, rather than introducing artificial circuit activity, this network manipulation restored normal biological network oscillatory activity (i.e., mirroring the brain state of the unstressed and resilient animals) and behavioral function. The findings generated using this approach provided evidence that stress-induced dysregulation of PFC-AMY circuitry disrupts the PFC-dependent synchronization of ultraslow limbic activity. Furthermore, this dysregulation

plays a key role in the manifestation of emotional behavior pathology in MDD.

## RESULTS

### PFC Delta and Beta Activity Influence Limbic Oscillations

To identify neural circuit components underlying susceptibility, we implanted 33 animals with microwire electrodes (Figure 1B): 19 of these mice were subjected to chronic social defeat stress, and 14 mice were used as non-stressed behavioral controls. The most established behavioral assay for measuring the impact of chronic social defeat stress in mice is the single-chamber social interaction test (hereafter referred to as the "choice interaction test") (Golden et al., 2011). In this assay, the interaction ratio is defined as the total time an animal remains proximal to a CD1-strain mouse in a small chamber divided by the time spent proximal to that same chamber when it is empty. The interaction ratio has been validated as a behavioral measure of susceptibility or resilience to chronic social defeat, with susceptible mice exhibiting interaction ratios less than one (Krishnan et al., 2007). As expected, implanted mice subjected to chronic social defeat stress exhibited lower interaction ratios during the choice interaction test compared to control animals ($p = 0.03$ using rank-sum test; Figure 1C). Furthermore, both susceptible and resilient animals were identified in the stressed group of implanted mice (Figure 1C). Together, these results confirmed that mice implanted with recording electrodes continue to show normal behavioral responses to chronic stress. To discover the neural network state that accompanied stress susceptibility, we directly measured the impact of CD1 exposure on LFP activity in chronically stressed mice using the FIT assay (Figure 1A). Critically, this assay allows for the direct quantification of circuit responses to an aggressor mouse without the influence of the exploratory or escape behaviors exhibited during the choice interaction test (Kumar et al., 2014).

Given that dysregulation of PFC-dependent circuits has been implicated in contributing to MDD, we focused on PFC as the seed region to perform functional connectivity analysis. We initially sought to define which oscillatory frequency bands to investigate by determining those that were PFC driven. We took advantage of prior studies that suggest that directional interactions across brain circuits can be extracted from phase relationships between concurrently recorded LFP signals (Dzirasa et al., 2013; Narayanan et al., 2011). We found that AMY, NAc, and VTA oscillatory activities were particularly influenced by PFC within the delta (2–7 Hz) range (Figures 1D–1F) during exposure to the CD1 mouse. Beta (14–23 Hz) activity in the AMY was sensitive to PFC input as well (Figures 1E and 1F). Thus, PFC activity influenced limbic delta and beta oscillations, suggesting that PFC delta and beta oscillations could be used as the seed for our functional connectivity analysis.

### PFC Synchronizes Slow-Evolving Limbic Beta Dynamics

Next, we probed the relationship between PFC oscillations within these PFC-leading frequency bands (delta and beta) and LFP activity measured across the limbic regions. LFP power reflects global activity patterns within a given brain region, while LFP coherence quantifies the extent to which two distinct brain regions oscillate together across time. As such, LFP coherence reflects brain circuit activity (Igarashi et al., 2014; Jones and Wilson, 2005). To quantify activity across the cortico-limbic network, we calculated LFP power within each of the four brain regions and LFP coherence between the six pairs of brain regions we recorded. Since the dysfunctional networks previously uncovered in MDD using fMRI show slow-evolving oscillatory periods that are more than 1 s (ultraslow; <1 Hz) (Greicius et al., 2007; Sheline et al., 2010), power and coherence were measured using 1 s temporal windows. This approach allowed us to identify the ultraslow patterns by which these measures change over extended periods of time (Figures 2A and 2B). We then determined the extent to which PFC activity correlated with each measure of limbic brain activity (18 measures in this study; there were 3 power measures and 6 coherence measures for each of the two PFC-dependent frequency bands) over the recording period (Figures 2B and 2C). Nearly all of the power and coherence measures we tested showed correlated activity with PFC ($p < 0.05$ for 341/342 comparison of 18 correlations/animal using Spearman rank; $N = 19$ animals; $p = 0.06$ for the remaining NAc-VTA coherence circuit measure from one animal; Figure 2C), aligning with fMRI studies that show widespread functional connectivity between PFC and limbic regions (Sheline et al., 2010). After confirming that our approach quantified functional connectivity in mice using PFC as the seed region, we used the raw correlation measures obtained from each implanted animal as the parameters for a network analysis aimed at identifying the neural architecture underlying the stress-susceptible state.

### Modeling Depression Network Dysfunction Using Chronic Social Defeat Stress

To infer a "depression network" model that described the manifestation of the susceptible phenotype, we assayed coherence and power parameters during the FIT. A FIT reactivity score is defined as the difference in each measure between when the CD1 is and is not present ($X_{FIT} = X_{CD1} - X_{Emypty}$; Figure 3A). We have shown previously that the PFC LFP-power reactivity score predicts susceptibility to social defeat stress in stress-naive mice (Kumar et al., 2014). Here we used the FIT assay to directly quantify the extent to which an acute exposure to a CD1 impacts neural circuit function within limbic regions and frequencies that we found to be PFC directed (Figure 3A).

We determined the contribution of the 18 neural circuit measures obtained for each animal to its individual behavioral responses using a machine learning approach, the elastic net (Zou and Hastie, 2005). This multivariate regularized regression method tests the relationship between the 18 circuit-reactivity values measured during the FIT (i.e., change in $R^2$ values; $X_{1...n}$) and the behavioral interaction ratio measured during the choice interaction test ($Y_{1...n}$). It infers a network model that explains the emergence of stress susceptibility. All circuit features retained in the network model contribute to the network, and because each of the circuit features is tested within a single multivariate model, there is no need for classical corrections for multiple comparisons. In our case, only one circuit feature

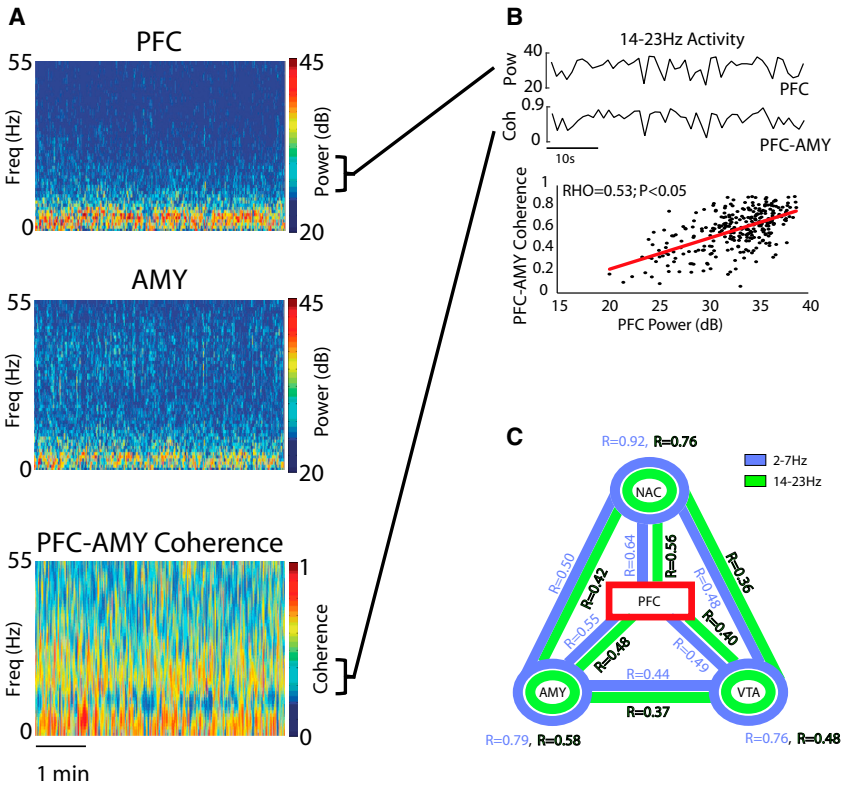


**Figure 2. Limbic Network Dynamics Exhibit Functional Connectivity with PFC**

(A) Spectral plots showing PFC and AMY activity, and the coherence between the two regions (top). Sample time course trace of PFC power and PFC-AMY coherence in the 14–23 Hz band (bottom).

(B) Correlation between PFC power and PFC-AMY coherence in a representative mouse. Each point corresponds to 1 s of LFP activity recorded during the 5 min session ($p < 0.01$, $R = 0.53$ using Spearman rank correlation; top).

(C) Functional connectivity using PFC-seed analysis. RHO values were calculated using Spearman rank between PFC power and limbic power (circles) or coherence (links). Values shown on the plot were averaged across 33 mice. $p < 0.05$ for all seed comparisons, with the exception of one measure (NAc-VTA; $p = 0.06$).

was retained in the model, converging on the solution of a univariate regression.

The interaction ratio measured for each mouse's behavior was directly and specifically related to the correlation between PFC power and AMY-VTA coherence in the beta oscillatory band during the FIT (Figure 3B; hereafter referred to as "P-AV" network). Exposure to the CD1 mouse decreased the correlation between PFC beta power and AMY-VTA beta coherence in the susceptible mice ((−)reactivity in the P-AV network) and increased this correlation in the resilient animals ((+)reactivity in the P-AV network; Figure 3C; $p < 0.05$; $R = 0.58$ using Pearson correlation). Notably, only the P-AV beta circuit reactivity measure was retained in the model, suggesting that reactivity in this network explained the susceptible phenotype independently of the other 17 neural measures we tested. Neither reactivity in PFC beta power nor AMY-VTA beta coherence alone correlated with the interaction ratio during social interaction testing (Figure 3D). Thus, P-AV reactivity did not simply reflect a global increase or decrease in PFC power or AMY-VTA coherence induced by exposure to the CD1; rather, P-AV reactivity directly reflected changes in the dynamics that coordinated these two measures across time.

## PFC Neurons Signal Synchrony between AMY and VTA

Since our depression network model suggested that PFC activity was causally linked to beta (14–23 Hz) coherence between AMY and VTA, we set out to determine if PFC unit firing signaled the synchronization of beta oscillations in AMY and VTA. We compared the firing of 169 PFC neurons recorded during the FIT to the instantaneous phase of AMY and VTA beta oscillations using phase-locking analysis (Figure 4A, top). With this approach, we found that 37/169 PFC neurons phase locked to AMY beta oscillations (Figure 4A, bottom) and that 33/169 neurons phase locked to VTA beta oscillations (Figure 4A, bottom). Finally, we found that 21/169 PFC neurons phase locked to beta oscillations in both AMY and VTA (Figure 4A). Thus, the data suggest that the coupling between AMY and VTA beta oscillations can be signaled by the firing of PFC neurons.

PFC phase locking to both AMY and VTA oscillations provides one putative mechanism whereby PFC could regulate AMY-VTA coherence. Nevertheless, there are other possible regulatory mechanisms. Specifically, PFC neurons could fire relative to the instantaneous relationship between oscillatory activity in AMY and VTA (rather than relative to the instantaneous phase of oscillations in each area; phase locking). To probe for such a mechanism, we quantified the phase offset between AMY and VTA beta oscillations at the instant each PFC neuron fired.

Since the phase offset time series between AMY and VTA was not uniformly distributed (Figure 4A), we expected that PFC neurons would also tend to fire at a non-uniform phase offset between AMY and VTA (i.e., mean resultant length [MRL] of the circular vector >0; see Figure 4B). To compare the actual firing of PFC neurons to the expectations based on purely random timing we (1) randomly sampled the AMY-VTA phase offset time series an equivalent number of times that a PFC neuron fired, (2) grouped these randomly sampled phase offsets and calculated their MRL, and (3) repeated this process 100,000 times, yielding a chance MRL distribution for that neuron. We then compared the phase offsets at which the PFC neurons actually fired to this random distribution. Neurons that exhibited MRL values outside of the 95% confidence interval of their chance MRL distribution were classified as synchrony ("SYNC") cells (Figure 4B). SYNC cells thus represent neurons that fire according to specific AMY-VTA phase offsets (compared against a random population of offsets that occur by chance).

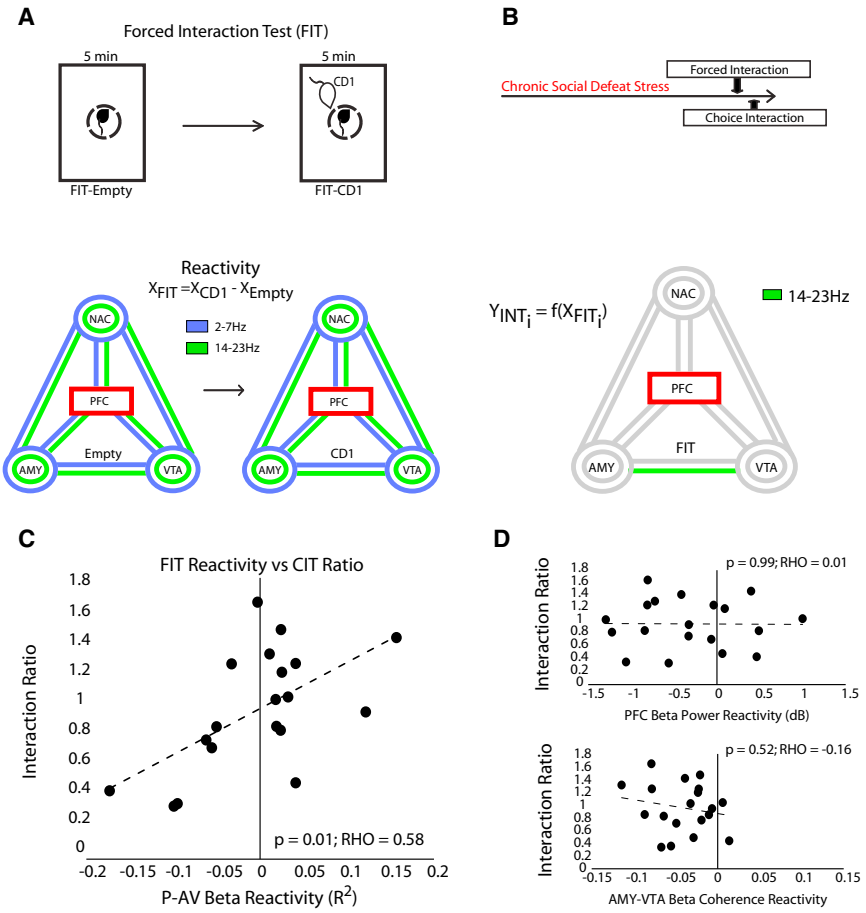


**Figure 3. PFC-Centered Network Dynamics Signal Stress Susceptibility**

(A) The PFC-centered FIT reactivity was compared to the choice interaction ratio using the elastic network. The PFC seed plot shows the 18 model parameters used for analysis (three power measures shown as circles and six coherence measures shown as lines for each of the two PFC-dependent frequencies bands).

(B) Only the PFC beta (14–23 Hz) power versus AMY-VTA beta coherence correlation was retained in the model.

(C) The correlation between these values is shown below (p = 0.01 using Spearman rank correlation; bottom).

(D) The mean PFC beta power and mean AMY-VTA beta coherence were calculated for each segment of the FIT, and the reactivity of each measure was compared to the choice interaction test ratio using a Spearman rank regression. There was no significant relationship between behavioral responses and either brain measure.

Nearly 23% (38/169) of PFC neurons fired relative to the phase offset between AMY and VTA (phase-offset locking; Figures 4B and 4C). The majority of SYNC cells (22/38) increased their firing when oscillatory activity in AMY and VTA was highly synchronized (+SYNC; neuronal firing increased at the dominant phase offset between AMY and VTA oscillations), while 16/38 of these SYNC cells increased their firing rate when AMY and VTA beta oscillations were desynchronized (−SYNC; neuronal firing increased at the non-dominant phase offset between AMY and VTA oscillations). Strikingly, the majority of SYNC cells did not phase lock to AMY or VTA beta oscillations, and the majority of PFC neurons that phase locked to AMY and VTA oscillations were not SYNC cells (Figure 4C, bottom).

Prior studies that probe spike-LFP relationships have shown that assessing the timing relationship between the two, using the introduction of temporal offsets between spikes and LFPs as part of the analysis, can clarify the mechanisms underlying spike-LFP interactions (Kumar et al., 2014; Siapas et al., 2005; Sigurdsson et al., 2010). Thus, we exploited this approach to probe the temporal mechanisms underlying the activity of SYNC cells (Figure 4D). We introduced temporal offsets ranging from −1 s to 1 s in 100 ms steps into our LFP analyses and recalculated the coupling between PFC activity and AMY-VTA synchrony in each of these shifted timeframes. The directionality of activity between PFC neuron firing and AMY-VTA was determined by the temporal offsets at which the coupling was observed. Strikingly, we found that the majority of SYNC cells fired relative to AMY-VTA synchrony 100 ms in the past (Figure 4D, top), indicating a strong relationship between SYNC cell firing and AMY-VTA synchrony in the immediate past. In contrast, few SYNC cells fired relative to the AMY-VTA synchrony measured at temporal offsets further in the past (6/38, 15%), demonstrating that phase-offset locking reflected a neural mechanism that was coordinated on a sub-second timescale. Nearly half of the SYNC cells fired relative to the synchrony observed 300 ms in the future (17/38, 45%). The majority of cells that fired relative to AMY-VTA synchrony in the future were +SYNC cells (i.e., the firing of these cells signaled an increase in synchrony). Together, our findings show that both types of SYNC cells detect AMY-VTA synchrony levels in the immediate past, and that +SYNC cells also predict increases in AMY-VTA synchrony in the immediate future. Notably, these findings also demonstrated that phase locking and phase-offset locking were both distinct mechanisms whereby the activity of PFC neurons could signal AMY and VTA synchrony. Nearly 50% (78/169) of PFC neurons exhibited at least one of these mechanisms.

## Direct PFC Stimulation Is Sufficient to Increase AMY-VTA Synchrony

Our results so far confirm that PFC neurons signaled the synchronization of AMY-VTA oscillations. To test whether PFC activation was sufficient to cause coherence between AMY and VTA, we implanted transgenic mice engineered to express channelrhodopsin-2 in layer V pyramidal neurons of cortex with recording electrodes in AMY and VTA, and a stimulating fiber in PFC (Figure 4E). We then recorded LFP activity during direct

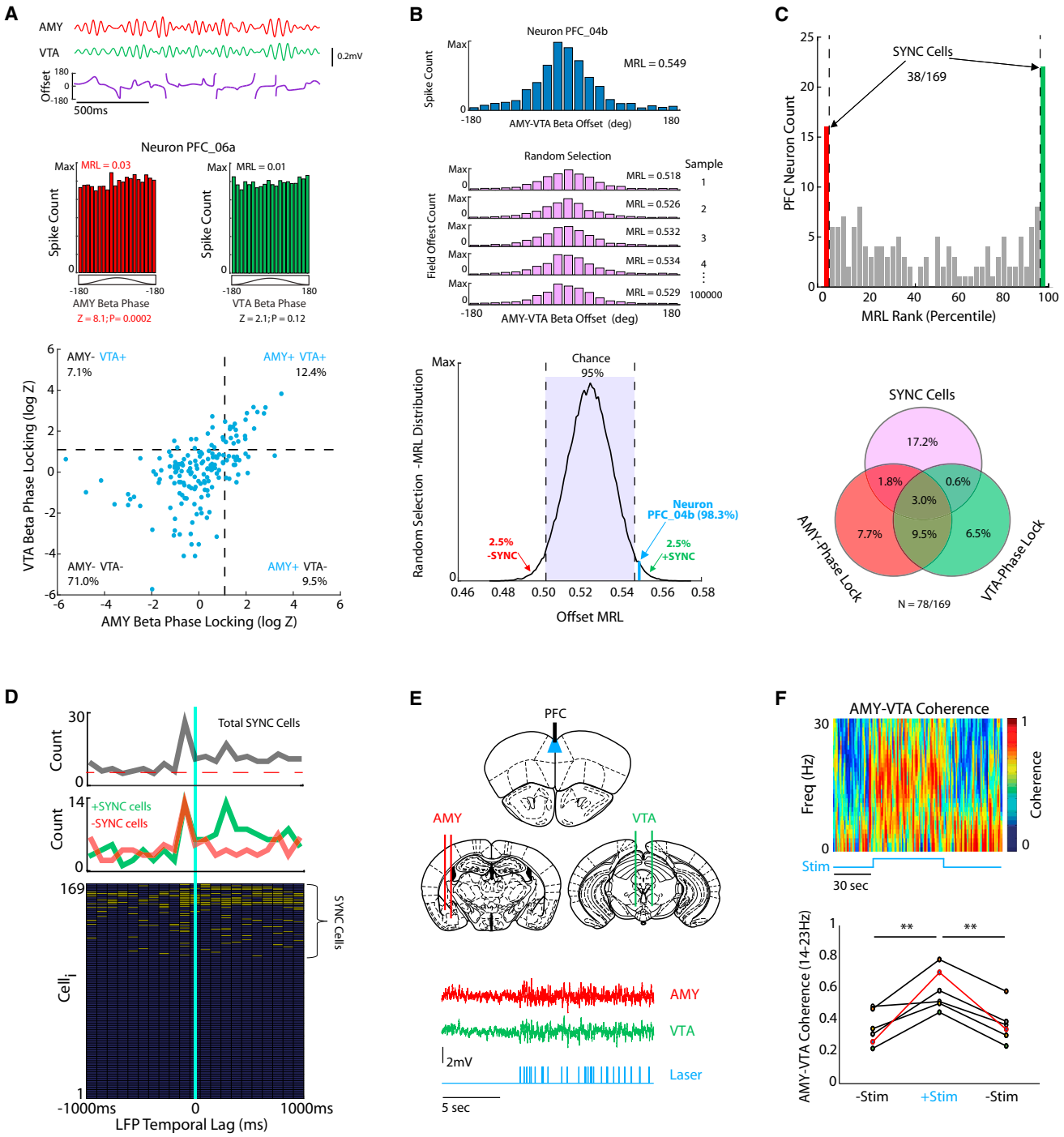


**Figure 4. PFC Activity Synchronizes AMY and VTA Beta Oscillations**

(A) Traces show beta-filtered LFP activity recorded from AMY and VTA during FIT, and their phase offset time series (top). Histograms depict the instantaneous LFP beta oscillatory phases at which an example neuron fires (middle). This example PFC neuron phase locked to AMY (left), but not VTA beta oscillations (right; $p < 0.05$ using the Rayleigh test of circular uniformity, where $Z = -\log|p|$). Rayleigh statistics (Z) for all neurons recorded during the FIT (N = 169 PFC neurons; bottom). The dashed lines correspond with the significance threshold for phase locking to AMY and/or VTA beta oscillations.

(B) Histogram depicting the distribution of instantaneous phase offsets between AMY and VTA beta oscillations when an example neuron fires, and the corresponding mean resultant length (MRL; top). The AMY-VTA phase offset time series was randomly sampled the same number of times this neuron fired, yielding a chance MRL. Bootstrapping was repeated $10^5$ times to create a distribution of chance MRL values for the neuron (bottom).

(C) Neurons that exhibited MRL values outside of the 95% confidence interval of their chance MRL distribution were classified as synchrony (SYNC) cells. Venn diagram indicates the number of units that significantly phase lock to AMY and VTA oscillations, and to the offset between them (SYNC cells).

*(legend continued on next page)*

stimulation of PFC with a pre-recorded PFC spike pattern (mean stimulation rate of 4.02 Hz for 60 s; see Figure 4E). Direct stimulation of the subcortical projections in PFC significantly increased beta synchrony between AMY and VTA (Figure 4F). Thus, PFC firing was indeed sufficient to increase AMY-VTA coherence. Together, these findings demonstrated a definitive physiological link between PFC activity and AMY-VTA coherence. The correlation between PFC beta power and AMY-VTA coherence in stressed animals is not simply a network epiphenomenon. Rather, the correlation between these two neural measures reflected an emergent property of a PFC-regulated physiological network (P-AV network).

## PFC-AMY Circuit Stimulation Reverses Network and Behavioral Phenotype Induced by Chronic Stress

We next sought additional evidence of causality by manipulating the P-AV network in chronically stressed "susceptible" mice and measuring their behavioral response. Importantly, we sought to restore normal healthy function to the circuit. We targeted the PFC-AMY axis of the circuit because our LFP directionality analysis suggested that PFC exhibited a direct influence on AMY (but not VTA) activity in the beta frequency band, justifying the connection between PFC and AMY as a putative target for manipulating the P-AV network in a manner consistent with the endogenous network function that already exists.

To modulate PFC-AMY circuit activity, we used a chemogenetic approach based on DREADDs. These DREADDs are variants of muscarinic receptors (−hM3D) that have been modified to be selectively activated by the pharmacologically inert compound, clozapine-*N*-oxide (CNO). When activated by CNO, hM3D increases the likelihood of neuronal firing through signaling by the G protein Gq (Alexander et al., 2009; Armbruster et al., 2007). To specifically target neurons within the PFC-AMY circuit, we used an intersectional approach described in the Experimental Procedures. This strategy was designed to yield expression of the DREADDs in AMY neurons that form synaptic connections with neurons in PFC (i.e., both afferent and efferent connections; see Figures 5A and 5B) (Gradinaru et al., 2010) (Figure S2). Next, we evaluated amygdalar cell types impacted by the DREADDs by measuring CNO-dependent evoked postsynaptic currents in slices from these mice. Activation of the Gq-DREADDs by CNO reversibly enhanced both evoked excitatory postsynaptic currents (eEPSCs) and $GABA_A$-evoked inhibitory postsynaptic currents (eIPSCs) in AMY principal neurons (Figures 5C and 5D; see also Figure S3), implying that the DREADDs were expressed in both excitatory pyramidal neurons and inhibitory GABAergic interneurons. The evoked IPSCs were completed blocked by bath application of 10 μM bicuculline methiodine, indicating that the IPSCs were mediated by $GABA_A$ receptors. Thus, our targeting strategy successfully rendered the cells in AMY that formed connections with PFC more likely to fire in response to excitatory input (PFC-AMY circuit stimulation).

Next, we examined the network-level effects of DREADD stimulation in vivo. Mice were virally manipulated using our targeting strategy and either subjected to chronic social defeat stress or used as unstressed controls. Following chronic social defeat stress, stressed mice and the non-stressed controls were implanted with recording electrodes in AMY, PFC, and VTA. After surgical recovery, mice were treated with vehicle (i.p., intraperitoneally) and neurophysiological data were collected during a FIT. Twenty-four hours later, mice were treated with CNO (i.p.) to induce DREADD activation, and the FIT was repeated (Figure 6A).

During the initial forced interaction testing session, exposure to the CD1 mouse reduced connectivity in the P-AV network (e.g., a decrease in correlation between PFC power and AMY-VTA coherence; (−)reactivity) in all of the vehicle-treated, stress-susceptible mice (N = 8; Figure 6B). In stressed, susceptible animals, PFC-AMY circuit activation with CNO selectively attenuated P-AV network (−)reactivity, such that animals exhibited a smaller decrease in the correlation between PFC beta power and AMY-VTA beta coherence in response to the CD1 exposure. In non-stressed control animals, treatment with CNO potentiated P-AV network (−)reactivity. In the resilient mice, CNO had no impact (N = 6 mice; Figure 6B). Critically, there was no difference in P-AV network (−)reactivity in uninfected susceptible mice subjected to repeat FIT testing ($p = 0.84$ using rank-sum test; see Figure S4), demonstrating that activation of the PFC-AMY circuit (and not simply repeat FIT testing) suppressed the "susceptible-network" phenotype we identified in chronically stressed mice. Control animals on CNO showed reactivity that resembled the susceptible animals on vehicle, and susceptible animals on CNO showed reactivity that resembled the resilient and unstressed animals on vehicle. Notably, stress-susceptible mice treated with vehicle tended to show (−)reactivity values that were more negative compared to the vehicle-treated, stress-resilient mice and the non-stressed controls ($p = 0.08$ and 0.05 using one-tailed rank-sum test; Figure 6B, bottom), providing additional biological support for the neural network-based model we inferred using machine learning in which (−)reactivity signaled susceptibility.

Since the DREADD strategy reversed the "susceptible-network" neural phenotype in stressed mice (large P-AV reactivity), we hypothesized that activation of the PFC-AMY circuit might rescue their behavioral responses during the choice interaction test as well. We again used our viral infection strategy in mice with wheat-germ agglutinin (WGA)-Cre in PFC and Gq-DREADDs or GFP control in AMY. After recovery, mice were

(D) Phase-offset MRL values were calculated for PFC neurons at LFP temporal lags ranging from −1 s to 1 s in 100 ms steps, and SYNC cells were detected based on a 99.7619% confidence interval ($\alpha = 0.05/21$ bins). The majority of SYNC cells phase-offset locked to AMY-VTA synchrony 100 ms in the past. SYNC cells that fired at periods of high synchrony (+SYNC cells, green) also coupled to AMY-VTA synchrony 300 ms in the future. Plot below shows all PFC neurons at each of the temporal offsets we tested. Neurons that showed phase-offset locking at a given LFP temporal lag are shown in yellow.

(E) Experimental recording and stimulation sites for optogenetic experiment (top). LFP traces recorded from AMY and VTA during optogenetic stimulation of PFC (bottom). Light stimulation trace is shown below LFPs.

(F) PFC stimulation increased beta synchrony between AMY and VTA (**$p < 0.01$ using Friedman's test followed by sign-rank test). The animal in red corresponds with the coherence plot shown above.

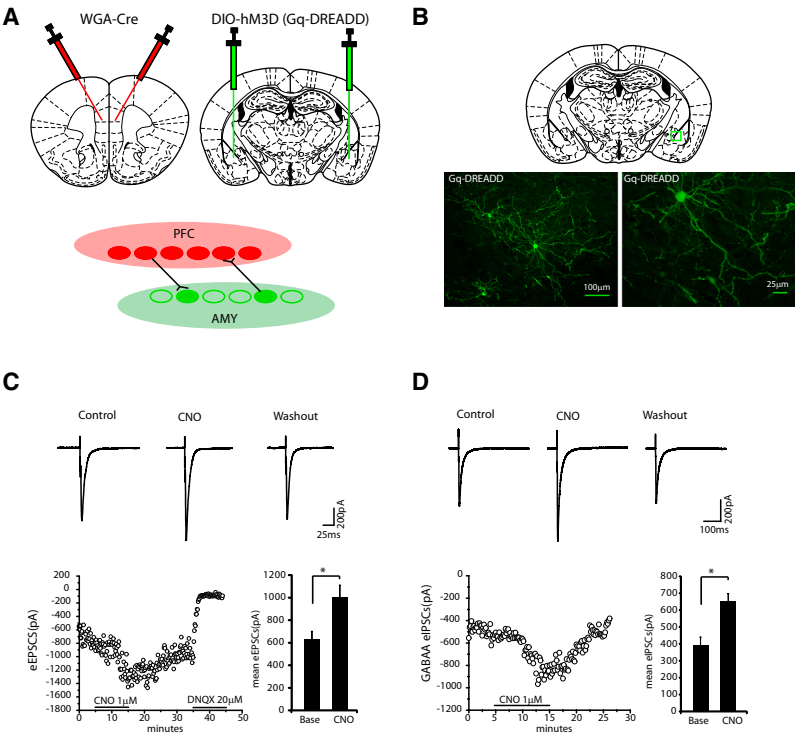


**Figure 5. In Vitro Confirmation of DREADD Stimulation**

(A) Schematic of viral infection strategy (top) designed to yield expression of Gq-DREADD in AMY neurons that form synaptic connections with PFC (bottom). *trans*-synaptic wheat-germ agglutinin (WGA)-tagged Cre was injected into the PFC, and floxed Gq-DREADD was injected into the AMY.

(B) Histology showing Gq-DREADD expression in AMY (green) using the viral targeting strategy described in (A).

(C) Activation of Gq-DREADD by CNO reversibly enhances AMPA-excitatory postsynaptic currents (EPSCs) in AMY principal neurons. Averaged traces of evoked EPSCs obtained during baseline, bath application of CNO (1 μM), and washout periods are shown (top). Time course of amplitude of evoked EPSCs during baseline, bath application of CNO (1 μM), washout, and bath application of DNQX (20 μM) (bottom left). CNO administration increased the peak mean evoked EPSCs (data were analyzed using two-tailed paired t test; $t_3 = 8.09$, *p = 0.004, N = 4 neurons; bottom right).

(D) Activation of Gq-DREADD by CNO reversibly augments $GABA_A$-inhibitory postsynaptic currents (IPSCs) in AMY principal neurons. Averaged traces of evoked IPSCs obtained during baseline, bath application of CNO (1 μM), and washout are shown (top). Time course of amplitude of evoked IPSCs during control, bath application of CNO (1 μM), and washout (bottom left). CNO administration increased the peak mean evoked IPSCs (data were analyzed using two-tailed paired t test; $t_5 = 7.66$, *p = 0.0006, N = 6 neurons; bottom right). These results demonstrated that the DREADDs were expressed in both excitatory pyramidal neurons and inhibitory GABAergic interneurons using this targeting strategy.

Data shown as mean ± SEM.

subjected to chronic subordination stress or pair-housed as non-stressed controls (Figure 7A). We initially identified susceptible mice by measuring social behavior using a three-chamber choice social interaction test (Figure 7B). We used this modified three-chamber design in order to avoid habituating animals to the standard chamber and ultimately cofounding the measured interaction ratio during subsequent testing. Based on prior studies (Covington et al., 2010), the animals that exhibited the lowest 60% of social interaction scores in the three-chamber interaction test were treated as susceptible (Figure 7B). Importantly, there was no difference in the distribution of interaction times between the DREADD- and GFP-infected groups of susceptible mice in the three-chamber test (p = 0.3088 using Kolmogorov-Smirnov test; Figure 7B, inset). Thus, simply expressing the DREADDs was not sufficient to alter the behavior of animals in the absence of CNO. Similarly, treatment with CNO did not impact social interaction behavior in mice that did not express the DREADD receptor (Figure S5). After identifying the susceptible animals, all of the experimental mice were tested in the standard single-chamber choice interaction test following CNO treatment to stimulate the DREADD (Figure 7C; see Supplemental Experimental Procedures for further description). Importantly, DREADD stimulation had no effect on the locomotor profiles displayed by either of the groups (Figure 7D).

GFP-expressing stressed mice (pooled susceptible and resilient animals) exhibited interaction ratios that were lower than the non-stressed controls (p = 0.024 using Kolmogorov-Smirnov test), demonstrating that the stressed animals exhibited the typical profile of behaviors that emerged following social defeat stress. Comparison of the interaction scores for the stressed DREADD-infected mice to their GFP-infected controls revealed that PFC-AMY stimulation increased social interaction in the stress-susceptible animals and had no effect in the stress-resilient mice (p = 0.027 and 0.96, respectively, using rank-sum test; Figure 7C). No differences in interaction ratios were observed between DREADD-expressing stressed mice (pooled susceptible and resilient animals) and their non-stressed GFP controls (p = 0.43 using Kolmogorov-Smirnov test), demonstrating that social behavior was normalized in the stressed DREADD-expressing mice. Interestingly, activation of the PFC-AMY circuit tended to reduce the interaction ratio in the non-stressed controls as well (p = 0.14 using Wilcoxon rank-sum test; Figure 7C). Thus, the behavioral responses induced by DREADD activation mirrored the neurophysiological responses we observed in each of the groups using in vivo recordings.

Finally, to ensure that the neurophysiological and behavioral responses observed in susceptible mice during PFC-AMY DREADD stimulation did not result simply from a DREADD-induced disruption of normal AMY activity, we repeated experiments in a new group of susceptible animals that expressed the Gq-DREADD in AMY in a non-circuit-selective manner (Figure S6). Treatment with CNO in animals expressing Gq-DREADD under a CaMKII-driven promoter in the AMY failed to restore normal social interaction behavior or P-AV reactivity in these

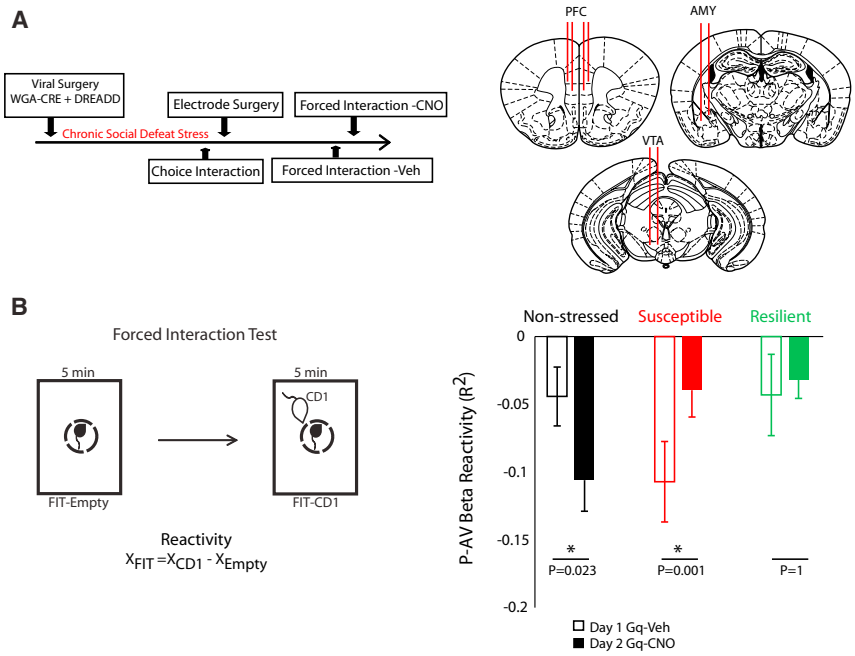


**Figure 6. PFC-AMY Stimulation Ameliorates Stress-Induced Network Adaptations**

(A) Schematic of experimental timeline (left) and electrode implantation sites (right).

(B) The correlation between PFC activity and AMY-VTA coherence (P-AV network) was quantified during each segment of the FIT (left). DREAAD activation potentiated the FIT reactivity in the P-AV network in non-stressed control mice, attenuated P-AV beta network reactivity in chronically stressed susceptible mice, and had no effect in the resilient mice (*$p < 0.05$ using sign-rank test; right). Data shown as mean ± SEM.

mice. Taken together, these data affirm our hypothesis that stimulation of the PFC-AMY circuit reverses the expression of the "susceptible" network and susceptible behavioral phenotypes after chronic social defeat stress in mice.

## DISCUSSION

Animal studies have been particularly useful in dissecting the neural circuit mechanisms underlying sleep, habit formation, spatial processing, fear, motor and sensory processing, and motivation (Crawley, 2007). Nevertheless, there have been several barriers to using rodents to model the emotional behavior changes that characterize psychiatric disorders (Nestler and Hyman, 2010). For example, it has simply not been feasible to model dysfunction across many of the behavioral domains observed in MDD, including guilt, mood, hallucinations, and suicidality. An alternative strategy for overcoming this hurdle is to create animal models that recapitulate the key disruptions in emotion networks that contribute to psychiatric disorders. Here we begin to identify and wield manipulations over such networks using a multidisciplinary approach including whole-circuit recordings, stress manipulations, behavioral analysis, machine learning, and direct brain stimulation using optogenetics to demonstrate that changes in specific PFC-regulated neural networks signal the emergence of behavioral dysfunction in a widely validated rodent model of depression. Furthermore, we provide direct evidence using DREADDs that normal emotional behavior is restored by reversal of a naturally occurring network-level disruption brought on by chronic stress. To our knowledge, this is the first demonstration of electrophysiological parallels between a key neural network-level phenotype observed in patients with MDD and emotional deficits in a preclinical model of the disorder. The preclinical model now affords us detailed and more comprehensive understanding of the specific real-time dynamics of network function that are not currently available in humans, thus uncovering novel targets for therapeutic development.

We began these studies with the well-recognized findings from both clinical and pre-clinical models that regulation of emotional behavior is highly dependent on the PFC. The PFC makes direct monosynaptic connections with multiple limbic brain regions, including AMY and VTA (Oh et al., 2014), and these PFC-dependent circuits have been shown to regulate anxiety (Likhtik et al., 2014), fear (Kumar et al., 2014), and psychomotor activity (Kim et al., 2015). Multiple studies have also implicated the dysregulation of PFC-dependent circuits as a central endophenotype of depression (Dzirasa et al., 2013; Greicius et al., 2007; Kumar et al., 2013; Mayberg et al., 1999; Salvadore et al., 2010; Sheline et al., 2010). Further, chronic antidepressant treatment reverses this neural circuit phenotype in the mouse model of depression (Dzirasa et al., 2013). We built on these findings in order to begin to dissect the distinct disruptions in emotion network critical for advancing understanding of psychiatric disorders. We now find that the emergence of behavioral pathology in a chronic stress-based model of MDD is associated with altered function across ultraslow PFC-dependent beta networks.

The studies presented here provide one of the first glimpses of large-scale network analysis that will be critical to unraveling the complex encoding of emotional processing. We identified the P-AV network, whereby susceptible responses are reflected in failure of coordination between PFC power and AMY-VTA coherence, using a data-driven strategy based in machine learning. The model solution generated by the elastic net is comprised of the non-zero coefficients that account best for the network recordings. Taken together, our behavioral, neurophysiological, and stimulation-based experiments provide strong support for the network model generated using our data-driven strategy.

On a cellular level, we show that nearly 50% of single units in the PFC neurons phase lock to oscillations in AMY and/or VTA, or to the phase offset between AMY and VTA oscillations (phase-offset locking; SYNC cells). To our knowledge, the identification of SYNC cells marks the first time that cortical activity has been shown to signal the phase offset between spatially distinct subcortical oscillations. Directionality studies of the

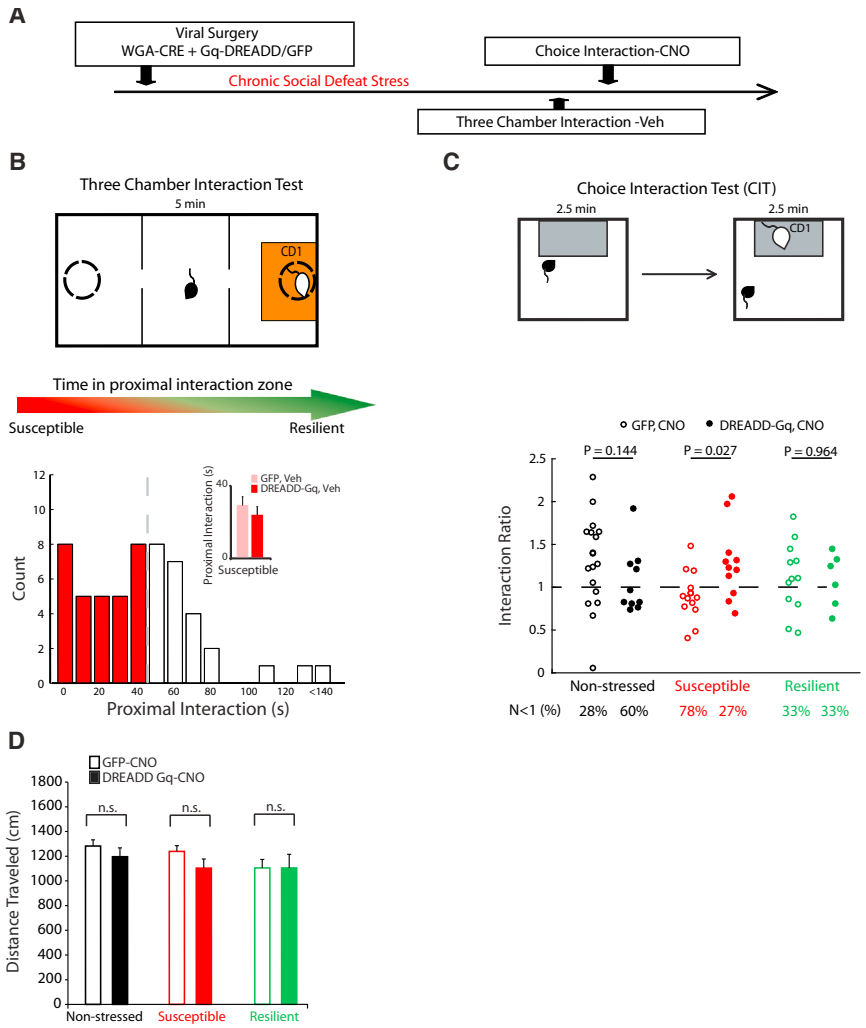


**Figure 7. PFC-AMY Stimulation Reverses Stress-Induced Behavioral Deficits**

(A and B) (A) Schematic of experimental timeline and (B) three-chamber social interaction test (top). Distribution of proximal interaction scores during post-stress three-chamber social interaction test (top; N = 55 mice). Similar interaction scores were observed between GFP and Gq-DREADD that displayed interaction scores within the lower 60% percentile ($p = 0.366$ using Wilcoxon rank-sum test; N = 11 and 14 for Gq-DREADD-susceptible and GFP, respectively; bottom).

(C) PFC-AMY activation increased social interaction in the stress-susceptible mice in the social interaction test ($p = 0.026$ using Wilcoxon rank-sum for comparison between DREADD-Gq- and GFP-expressing mice), and tended to reduce social interaction in the non-stressed control mice ($p = 0.14$). PFC-AMY stimulation had no effect in the resilient mice.

(D) No significant effects of viral vector (GFP versus Gq-DREADD; $F_{1,52} = 1.33$, $p = 0.25$; N = 10–18 mice per group) or viral vector × stress ($F_{1,52} = 0.1$, $p = 0.76$; N = 10–18 mice per group) were observed on gross locomotor behavior in the susceptible mice using two-way ANOVA.

Data shown as mean ± SEM.

phase-offset lock phenomenon indicated that the majority of SYNC cells phase-offset locked to limbic beta oscillatory activity 100 ms in the immediate past (i.e., AMY-VTA phase synchrony state preceded PFC firing), and nearly half of the SYNC cells also phase-offset locked to activity nearly 900 ms in the future (i.e., PFC firing preceded AMY-VTA phase synchrony state). Thus, SYNC cells may lie within a PFC-mediated feedback control circuit that detects and regulates the timing of sub-cortical oscillations to enable distinct network-level computations. This is consistent with our optogenetic findings, which showed that direct PFC activation was sufficient to increase the beta coherence between AMY and VTA. Our findings also raise the hypothesis that phase-offset locking may serve as a general brain mechanism whereby the cortex coordinates spatially distributed brain regions to promote emotional behavior.

PFC activity has been shown to signal safety in threatening environments (Adhikari et al., 2010). In animals that exhibit behavioral dysfunction after stress (e.g., susceptible mice), acute CD1 exposure disrupts the regulation of AMY and VTA interactions by PFC. Furthermore, direct stimulation of PFC-AMY circuitry using DREADDs normalizes activity in the P-AV beta network and restores behavioral function in susceptible mice. Thus, the coherence between AMY and VTA may assign salience to threat cues in order to signal risk during various emotion experiences. When this coherence signal is regulated by PFC, an animal can maintain its normal function under threatening conditions. Thus, our findings suggest that the P-AV network contributes to the emotion experiences that guide behavior. Our observations suggest that the relationship between P-AV reactivity and emotional regulation may lie along a U-shaped curve (Figure 8). The state of a given emotional network along this curve is modulated by PFC inputs to AMY since this PFC-AMY circuit is altered by chronic stress and direct stimulation of this circuitry using DREADDs. Given that deficits in functional connectivity across PFC-dependent networks have been described in MDD (Greicius et al., 2007; Nugent et al., 2015), activity across the P-AV network may serve as a novel translational measure of face validity in preclinical models of MDD.

Using circuit manipulation, we were able to restore the P-AV network in stressed animals to the natural state that occurs in unstressed animals under standard physiological conditions. Our viral infection strategy resulted in DREADD expression in inhibitory and excitatory neurons. The PFC makes direct projections on glutamatergic neurons and feedforward local inhibitory circuits in AMY (Ehrlich et al., 2009). Given that local inhibitory-excitatory circuits are critical to generating oscillatory activity (Bartos et al., 2007), this feedforward circuitry may play a central role in regulating local oscillatory timing, ultimately synchronizing

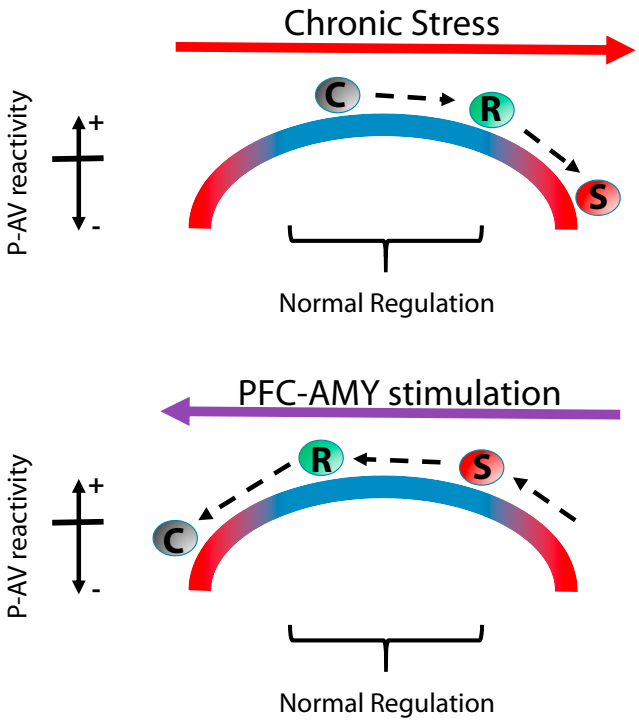


**Figure 8. Model of Stress Effects on P-AV Reactivity and Threat Regulation**

The relationship between P-AV reactivity and threat regulation can be modeled by the upside-down U-shaped curve that is common to many biological systems. Chronic stress drives the network state to the right such that P-AV reactivity decreases. Susceptible mice show the largest P-AV reactivity change and the largest behavioral dysregulation, while little differences in either measure are observed in resilient mice (top). Stimulation of the PFC-AMY circuit moves the network state to the left such that P-AV reactivity increases in susceptible mice, restoring normal reactivity and behavioral regulation. In the control mice, this manipulation destabilizes the normal network state and decreases P-AV reactivity (bottom).

AMY beta oscillations with efferent input from PFC. The susceptible brain state may then reflect the extent to which stress induces plasticity in these circuits. Our WGA-Cre viral targeting strategy also results in DREADD expression in AMY neurons that project to PFC. Many of these glutamatergic neurons also send axon collaterals to NAc (McDonald, 1991), providing cellular mechanisms whereby decreasing the input resistance of AMY neurons could potentially serve to coordinate large-scale subcortical limbic dynamics timed to PFC input.

Our DREADD manipulation directly targets the capacity of PFC to regulate AMY by increasing the likelihood of AMY neuronal firing in response to efferent input (ultimately decreasing the input resistance of excitatory PFC efferents). In the absence of novel closed-loop optogenetic protocols, which stimulate the brain timed to ongoing patterns of activity in PFC, even direct stimulation of PFC to AMY axon terminals would fail to achieve this type of regulation. For instance, optogenetic stimulation has been used to drive neurons based on their projection targets (Chaudhury et al., 2013; Stuber et al., 2011), and in this study we use a transgenic approach to selectively stimulate PFC efferents in layer V. Nevertheless, nearly all protocols for such open-loop optogenetic stimulation "override" the ongoing oscillatory dynamics that coordinate PFC output under physiological conditions, thus failing to restore the regulation of AMY activity by PFC dynamics. To this point, we show that exposure to a CD1 decreases AMY-VTA coherence in both the susceptible and resilient mice (see Figure 3B, bottom). Thus, it is the regulation of AMY-VTA coherence by PFC, and not AMY-VTA coherence itself per se, that underlies susceptibility. While multiple open-loop optogenetic stimulation protocols (including PFC layer V stimulation, as shown here) may increase AMY-VTA coherence, they would be unlikely to achieve the type of regulation necessary to correct the P-AV network dysfunction that defines the susceptible brain state. Indeed, there is a growing appreciation in the field that the timing, duration, and target and off-target effects from cellular manipulation are critical considerations for the interpretation of network and behavioral responses (Otchy et al., 2015).

Psychological stress is a major risk factor for the onset and exacerbation of MDD. Stress induces adaptations in cortical and limbic circuitry (Campioni et al., 2009; Dias-Ferreira et al., 2009; Ghosh et al., 2013; Kim et al., 1996; Yuen et al., 2012). For example, multiple distinct stress-induced cellular and molecular adaptations have been shown to regulate chronic social defeat syndrome in rodents. These adaptations include synaptic potentiation of thalamic inputs into NAc (Christoffel et al., 2015), $I_h$ current increases in VTA (Friedman et al., 2014), and gene expression changes in PFC (Covington et al., 2010; Vialou et al., 2014). Since manipulation of several distinct network nodes (circuits/brain areas) is sufficient to overcome these stress-induced cellular modifications to restore the normal emotional behavior (Bagot et al., 2015; Christoffel et al., 2015; Covington et al., 2010; Friedman et al., 2014), it is likely that these distinct molecular adaptations converge at the level of circuits or brain networks to yield the syndrome. Here we integrate the disparate neural sites involved in stress responses by showing how chronic stress alters the PFC-dependent coordination of long-range limbic networks to yield dysfunction in emotional behavior. Our findings suggest that a disruption in the capacity of PFC to coordinate neural interactions between AMY and VTA may be a central brain mechanism underlying MDD. Furthermore, therapeutics that directly target these network interactions may have the potential to rapidly ameliorate depression psychopathology.

## EXPERIMENTAL PROCEDURES

### Animal Care and Use

Studies were conducted with approved protocols from the Duke University Institutional Animal Care and Use Committee and were in accordance with the NIH guidelines for the Care and Use of Laboratory Animals. See Supplemental Experimental Procedures for additional details.

### Electrode Implantation Surgery

At an age of 6–7 weeks, C57 mice were anesthetized with isoflurane and placed in a stereotaxic device, and metal ground screws were secured to the cranium. A total of 32 tungsten microwires were arranged in array bundles and implanted in AMY (basolateral AMY and central extended AMY), NAc, PFC (prelimbic and infralimbic cortex), and VTA. See Supplemental Experimental Procedures for additional details. Histological analysis of implantation sites

was performed at the conclusion of experiments to confirm recording sites used for neurophysiological analysis (see Figure S7).

### Neurophysiological Data Acquisition

Headstages were connected without anesthesia 30 min prior to recording sessions. All neurophysiological recordings were performed during the FIT. Neuronal activity was sampled at 30 kHz using the Cerebus acquisition system (Blackrock Microsystems Inc.). LFPs were bandpass filtered at 0.5–250 Hz and stored at 1,000 Hz. Neurophysiological recordings were referenced to a ground wire connected to ground screws.

### Determination of LFP Oscillatory Power and Cross-Area Synchrony

Signals recorded from all of the implanted microwires were used for analysis. Using MATLAB (MathWorks), a sliding Fourier transform with Hamming window was applied to the LFP signal using a 1 s window and a 1 s step. Frequencies were analyzed with a resolution of 1 Hz. Additional analytical details are available in the Supplemental Experimental Procedures.

### Elastic Net Analysis

The spearman rank correlation coefficient was calculated between each limbic activity measure (three power measures and six coherence measures) and PFC power in the 2–7 Hz and 14–23 Hz range. FIT reactivity was then calculated for each of the 18 activity measures as $RHO^2_{(CD1)} - RHO^2_{(Empty)}$. The 18 calculated reactivity measures were used as observation variables, and the interaction scores measured during the choice interaction test were taken as the response at each observation.

The elastic net is a regularized regression method that solves the problem,

$$\min_{\beta_0 \beta} \left( \frac{1}{2N} \sum_{i=1}^{N} \left( y_i - \beta_0 - x_i^T \beta \right)^2 + \lambda P_\alpha(\beta) \right),$$

where

$$P_\alpha(\beta) = \frac{(1-\alpha)}{2} \| \beta \|_2^2 + \alpha \| \beta \|_1 = \sum_{j=1}^{p} \left( \frac{(1-\alpha)}{2} \beta_j^2 + \alpha |\beta_j| \right),$$

with $N$ the number of observations, $y_i$ the response at observation $i$, $x_i$ a vector of "feature" data (length p) at observation $i$, $\lambda$ a positive regularization parameter, $\beta_0$ a scalar "intercept," and $\beta$ coefficients on the different features (Zou and Hastie, 2005). The elastic net was solved using 10-fold cross validation and optimized based on the global minimum of the mean squared error with alpha values ranging from $10^{-6}$ to 0.9 incremented on a logarithmic scale. Data were analyzed using the MATLAB Machine Learning toolbox (MathWorks).

### Optogenetic Stimulation

The optogenetic experiment reflects additional analyses of data described in a previous experiment (Kumar et al., 2013). Briefly, B6.Cg-Tg(Thy1-ChR2/EYFP) 18Gfng/J were obtained from Jackson labs. Six 4- to 8-month-old heterozygous mice were implanted with a stimulating fiber in PFC, and recording electrodes in PFC, AMY, NAc, and VTA. Following surgical recovery, neurophysiological recordings were obtained while mice were stimulated in PFC using a pre-recorded PrL neuron spike pattern with a mean rate (4.02 Hz). Our physiology experiments were performed with a laser power of 2.5 mW, and the light fiber was located directly above the superior sagittal sinus.

### Viral Infusions

At an age of 6–7 weeks, C57 mice were anesthetized with ketamine (100 mg/kg) and xylazine (10 mg/kg), placed in a stereotaxic device, and injected with AAV-EF1a-mCherry-IRES-WGA-Cre (WGA-Cre) based on stereotaxic coordinates measured from bregma at the skull (PFC, 1.96 mm anterior-posterior [AP], ± 0.0.62 mm mediolateral [ML], and −2.28 mm dorsal-ventral [DV] at a 10° angle). Mice were also injected with AAV-hSyn-DIO-HA-hM3D(Gq)-IRES-mCitrine (Gq-DREADD) or AAV-hSyn-DIO-EGFP (GFP) based on stereotaxic coordinates measured from bregma (AMY, −1.46 mm AP, ± 2.9 mm ML, and −4.9 mm DV). A total of 0.5 μL of each virus was delivered bilaterally at each injection site over 5 min using a 5 μL Hamilton syringe. All viruses were obtained from the UNC Gene Therapy Center. Mice were singly housed for 2 weeks to allow for surgery recovery. Mice were then subjected to 15 days of chronic social defeat stress. Social interaction behaviors were tested with either the three-chamber social interaction test or the single-chamber social interaction test (see Supplemental Experimental Procedures for more details).

For in vivo neurophysiology experiments in virally infused animals, mice were implanted with microwire recording electrodes after chronic social defeat stress, as described above. It should be noted that these mice were anesthetized with isoflurane (1.5%); ketamine was not utilized in the post-chronic social defeat stress surgery given its antidepressant-like effects on chronic stressed mice (Donahue et al., 2014). At the completion of all behavioral and neurophysiological studies, mice were perfused transcardially with 4% PFA (EM Sciences), and brains were harvested, frozen, and sliced at 35 μm using a cryostat (Cryocut 1800, Reichert-Jung) and stained with an anti-GFP antibody at a dilution of 1:2,000 (rabbit polyclonal, A11122, Invitrogen) according to recommended Invitrogen protocol (see Supplemental Experimental Procedures). Fluorescence microscopy was used to identify both mCherry expression co-expressed with the WGA-Cre in PFC as well as FITC-stained mCitrine in the AMY using a Nikon Eclipse 80i fluorescence microscope. Confocal images were taken using a Zeiss LSM 510 inverted confocal microscope.

### Mouse Brain Slice Preparation for Single-Cell Recordings

Mice infected with Gq-DREADDs were deeply anesthetized with isoflurane. The brain was quickly removed from the skull after decapitation and immediately chilled in an ice-cold, oxygenated artificial cerebrospinal fluid (aCSF) solution containing 120 mM NaCl, 3.3 mM KCl, 25 mM $NaHCO_3$, 1.23 mM $NaH_2PO_4$ $H_2O$, 1.8 mM $CaCl_2$, 1.2 mM $MgSO_4$, and 10 mM glucose. Coronal slices (300 μm thickness) containing the AMY were cut with a moving blade microtome, and the slices were then kept in normal oxygenated aCSF at 35°C for 60 min. The slices were then kept at room temperature until used for recording.

A single slice was transferred to the recording chamber that was constantly perfused (~3 mL/min) with oxygenated aCSF at 35°C. The AMY principal neurons were viewed under a Zeiss upright microscope equipped with a 40× water immersion objective and an enhanced differential interference contrast (DIC) video microscope system. Recording electrodes with resistance of 4–8 MΩ were pulled from borosilicate glass capillaries (1.5 mm outside diameter [OD]) using a P97 electrode puller. Access resistance and input capacitance were electronically compensated by approximately 60%–70% and monitored throughout the experiment to confirm the stability of the recording. The internal pipette solution contained 130 mM CsCl, 4 mM NaCL, 0.2 mM EGTA, 4 mM Mg-ATP, 0.3 mM Tri-GTP, 10 mM HEPES, and 6 mM QX-314. The pH was adjusted to 7.4 with CsOH, and osmolarity was 290 mOsm. Signals were filtered at 5 kHz and were digitized at 10 kHz through a Digidata1440 interface controlled by pClamp10 software (Molecular Devices).

In all instances, EPSCs and IPSCs were initially recorded for 5 min to establish stable baseline values. Without altering the perfusion rate and temperature, the perfusion medium was then switched to one containing CNO (1 μM) for 10 min, followed by a drug washout. Synaptic responses were analyzed off-line using Clampfit 10 software (Molecular Devices). A paired t test was used to determine the statistical significance.

### Statistics

All data are presented as mean ± SEM unless otherwise specified.

## SUPPLEMENTAL INFORMATION

Supplemental Information includes Supplemental Experimental Procedures and seven figures and can be found with this article online at http://dx.doi.org/10.1016/j.neuron.2016.05.038.

## AUTHOR CONTRIBUTIONS

R.H., Q.L., K. Deisseroth, and K. Dzirasa designed experiments; R.H., S.D. Mague, B.M.K., N.M., L.K.D., R.C., S.K., and K. Dzirasa performed experiments; R.H., S.D. Mague, Q.L., B.M.K., N.M., L.L., J.W., L.K.D., C.B., R.C.,

L.C., D.D., S.D. Moore, and K. Dzirasa analyzed the data; R.H., S.D. Mague, Q.L., L.C., D.D., and K. Dzirasa wrote the paper. Detailed author contributions are provided in the Supplemental Information.

## ACKNOWLEDGMENTS

We would like to thank A. Talbot, S. Lisberger, M. Halassa, and R.A. Adcock for helpful comments on this manuscript; G. Feng and B.L. Roth for providing reagents; and Okechi Boms for technical support. This work was supported by funding from NIMH grants R37MH073853 and R01MH099192, and a DIBS Research Incubator award to K. Dzirasa. A special thanks to Freeman Hrabowski, Robert and Jane Meyerhoff, and the Meyerhoff Scholarship Program.

Received: November 4, 2015
Revised: April 21, 2016
Accepted: May 25, 2016
Published: June 23, 2016

## REFERENCES

Adhikari, A., Topiwala, M.A., and Gordon, J.A. (2010). Synchronized activity between the ventral hippocampus and the medial prefrontal cortex during anxiety. Neuron *65*, 257–269.

Alexander, G.M., Rogan, S.C., Abbas, A.I., Armbruster, B.N., Pei, Y., Allen, J.A., Nonneman, R.J., Hartmann, J., Moy, S.S., Nicolelis, M.A., et al. (2009). Remote control of neuronal activity in transgenic mice expressing evolved G protein-coupled receptors. Neuron *63*, 27–39.

Armbruster, B.N., Li, X., Pausch, M.H., Herlitze, S., and Roth, B.L. (2007). Evolving the lock to fit the key to create a family of G protein-coupled receptors potently activated by an inert ligand. Proc. Natl. Acad. Sci. USA *104*, 5163–5168.

Bagot, R.C., Parise, E.M., Peña, C.J., Zhang, H.X., Maze, I., Chaudhury, D., Persaud, B., Cachope, R., Bolaños-Guzmán, C.A., Cheer, J.F., et al. (2015). Ventral hippocampal afferents to the nucleus accumbens regulate susceptibility to depression. Nat. Commun. *6*, 7062.

Bartolomucci, A., and Leopardi, R. (2009). Stress and depression: preclinical research and clinical implications. PLoS ONE *4*, e4265.

Bartos, M., Vida, I., and Jonas, P. (2007). Synaptic mechanisms of synchronized gamma oscillations in inhibitory interneuron networks. Nat. Rev. Neurosci. *8*, 45–56.

Berton, O., McClung, C.A., Dileone, R.J., Krishnan, V., Renthal, W., Russo, S.J., Graham, D., Tsankova, N.M., Bolanos, C.A., Rios, M., et al. (2006). Essential role of BDNF in the mesolimbic dopamine pathway in social defeat stress. Science *311*, 864–868.

Campioni, M.R., Xu, M., and McGehee, D.S. (2009). Stress-induced changes in nucleus accumbens glutamate synaptic plasticity. J. Neurophysiol. *101*, 3192–3198.

Caspi, A., Sugden, K., Moffitt, T.E., Taylor, A., Craig, I.W., Harrington, H., McClay, J., Mill, J., Martin, J., Braithwaite, A., and Poulton, R. (2003). Influence of life stress on depression: moderation by a polymorphism in the 5-HTT gene. Science *301*, 386–389.

Chaudhury, D., Walsh, J.J., Friedman, A.K., Juarez, B., Ku, S.M., Koo, J.W., Ferguson, D., Tsai, H.C., Pomeranz, L., Christoffel, D.J., et al. (2013). Rapid regulation of depression-related behaviours by control of midbrain dopamine neurons. Nature *493*, 532–536.

Christoffel, D.J., Golden, S.A., Walsh, J.J., Guise, K.G., Heshmati, M., Friedman, A.K., Dey, A., Smith, M., Rebusi, N., Pfau, M., et al. (2015). Excitatory transmission at thalamo-striatal synapses mediates susceptibility to social stress. Nat. Neurosci. *18*, 962–964.

Covington, H.E., 3rd, Lobo, M.K., Maze, I., Vialou, V., Hyman, J.M., Zaman, S., LaPlant, Q., Mouzon, E., Ghose, S., Tamminga, C.A., et al. (2010). Antidepressant effect of optogenetic stimulation of the medial prefrontal cortex. J. Neurosci. *30*, 16082–16090.

Crawley, J.N. (2007). What's Wrong With My Mouse?: Behavioral Phenotyping Of Transgenic And Knockout Mice, Second Edition (John Wiley & Sons, Inc.).

Dias-Ferreira, E., Sousa, J.C., Melo, I., Morgado, P., Mesquita, A.R., Cerqueira, J.J., Costa, R.M., and Sousa, N. (2009). Chronic stress causes frontostriatal reorganization and affects decision-making. Science *325*, 621–625.

Donahue, R.J., Muschamp, J.W., Russo, S.J., Nestler, E.J., and Carlezon, W.A., Jr. (2014). Effects of striatal ΔFosB overexpression and ketamine on social defeat stress-induced anhedonia in mice. Biol. Psychiatry *76*, 550–558.

Dzirasa, K., Kumar, S., Sachs, B.D., Caron, M.G., and Nicolelis, M.A. (2013). Cortical-amygdalar circuit dysfunction in a genetic mouse model of serotonin deficiency. J. Neurosci. *33*, 4505–4513.

Ehrlich, I., Humeau, Y., Grenier, F., Ciocchi, S., Herry, C., and Lüthi, A. (2009). Amygdala inhibitory circuits and the control of fear memory. Neuron *62*, 757–771.

Friedman, A.K., Walsh, J.J., Juarez, B., Ku, S.M., Chaudhury, D., Wang, J., Li, X., Dietz, D.M., Pan, N., Vialou, V.F., et al. (2014). Enhancing depression mechanisms in midbrain dopamine neurons achieves homeostatic resilience. Science *344*, 313–319.

George, M.S., Lisanby, S.H., Avery, D., McDonald, W.M., Durkalski, V., Pavlicova, M., Anderson, B., Nahas, Z., Bulow, P., Zarkowski, P., et al. (2010). Daily left prefrontal transcranial magnetic stimulation therapy for major depressive disorder: a sham-controlled randomized trial. Arch. Gen. Psychiatry *67*, 507–516.

Ghosh, S., Laxmi, T.R., and Chattarji, S. (2013). Functional connectivity from the amygdala to the hippocampus grows stronger after stress. J. Neurosci. *33*, 7234–7244.

Golden, S.A., Covington, H.E., 3rd, Berton, O., and Russo, S.J. (2011). A standardized protocol for repeated social defeat stress in mice. Nat. Protoc. *6*, 1183–1191.

Gradinaru, V., Zhang, F., Ramakrishnan, C., Mattis, J., Prakash, R., Diester, I., Goshen, I., Thompson, K.R., and Deisseroth, K. (2010). Molecular and cellular approaches for diversifying and extending optogenetics. Cell *141*, 154–165.

Greicius, M.D., Flores, B.H., Menon, V., Glover, G.H., Solvason, H.B., Kenna, H., Reiss, A.L., and Schatzberg, A.F. (2007). Resting-state functional connectivity in major depression: abnormally increased contributions from subgenual cingulate cortex and thalamus. Biol. Psychiatry *62*, 429–437.

Igarashi, K.M., Lu, L., Colgin, L.L., Moser, M.B., and Moser, E.I. (2014). Coordination of entorhinal-hippocampal ensemble activity during associative learning. Nature *510*, 143–147.

Jones, M.W., and Wilson, M.A. (2005). Theta rhythms coordinate hippocampal-prefrontal interactions in a spatial memory task. PLoS Biol. *3*, e402.

Kendler, K.S., Karkowski, L.M., and Prescott, C.A. (1999). Causal relationship between stressful life events and the onset of major depression. Am. J. Psychiatry *156*, 837–841.

Kim, J.J., Foy, M.R., and Thompson, R.F. (1996). Behavioral stress modifies hippocampal plasticity through N-methyl-D-aspartate receptor activation. Proc. Natl. Acad. Sci. USA *93*, 4750–4753.

Kim, I.H., Rossi, M.A., Aryal, D.K., Racz, B., Kim, N., Uezu, A., Wang, F., Wetsel, W.C., Weinberg, R.J., Yin, H., and Soderling, S.H. (2015). Spine pruning drives antipsychotic-sensitive locomotion via circuit control of striatal dopamine. Nat. Neurosci. *18*, 883–891.

Krishnan, V., Han, M.H., Graham, D.L., Berton, O., Renthal, W., Russo, S.J., Laplant, Q., Graham, A., Lutter, M., Lagace, D.C., et al. (2007). Molecular adaptations underlying susceptibility and resistance to social defeat in brain reward regions. Cell *131*, 391–404.

Kumar, S., Black, S.J., Hultman, R., Szabo, S.T., DeMaio, K.D., Du, J., Katz, B.M., Feng, G., Covington, H.E., 3rd, and Dzirasa, K. (2013). Cortical control of affective networks. J. Neurosci. *33*, 1116–1129.

Kumar, S., Hultman, R., Hughes, D., Michel, N., Katz, B.M., and Dzirasa, K. (2014). Prefrontal cortex reactivity underlies trait vulnerability to chronic social defeat stress. Nat. Commun. *5*, 4537.

Likhtik, E., Stujenske, J.M., Topiwala, M.A., Harris, A.Z., and Gordon, J.A. (2014). Prefrontal entrainment of amygdala activity signals safety in learned fear and innate anxiety. Nat. Neurosci. *17*, 106–113.

Mayberg, H.S., Liotti, M., Brannan, S.K., McGinnis, S., Mahurin, R.K., Jerabek, P.A., Silva, J.A., Tekell, J.L., Martin, C.C., Lancaster, J.L., and Fox, P.T. (1999). Reciprocal limbic-cortical function and negative mood: converging PET findings in depression and normal sadness. Am. J. Psychiatry *156*, 675–682.

Mayberg, H.S., Lozano, A.M., Voon, V., McNeely, H.E., Seminowicz, D., Hamani, C., Schwalb, J.M., and Kennedy, S.H. (2005). Deep brain stimulation for treatment-resistant depression. Neuron *45*, 651–660.

McDonald, A.J. (1991). Organization of amygdaloid projections to the prefrontal cortex and associated striatum in the rat. Neuroscience *44*, 1–14.

Narayanan, V., Heiming, R.S., Jansen, F., Lesting, J., Sachser, N., Pape, H.C., and Seidenbecher, T. (2011). Social defeat: impact on fear extinction and amygdala-prefrontal cortical theta synchrony in 5-HTT deficient mice. PLoS ONE *6*, e22600.

Nestler, E.J., and Hyman, S.E. (2010). Animal models of neuropsychiatric disorders. Nat. Neurosci. *13*, 1161–1169.

Nugent, A.C., Robinson, S.E., Coppola, R., Furey, M.L., and Zarate, C.A., Jr. (2015). Group differences in MEG-ICA derived resting state networks: application to major depressive disorder. Neuroimage *118*, 1–12.

Oh, S.W., Harris, J.A., Ng, L., Winslow, B., Cain, N., Mihalas, S., Wang, Q., Lau, C., Kuan, L., Henry, A.M., et al. (2014). A mesoscale connectome of the mouse brain. Nature *508*, 207–214.

Otchy, T.M., Wolff, S.B., Rhee, J.Y., Pehlevan, C., Kawai, R., Kempf, A., Gobes, S.M., and Ölveczky, B.P. (2015). Acute off-target effects of neural circuit manipulations. Nature *528*, 358–363.

Salvadore, G., Cornwell, B.R., Sambataro, F., Latov, D., Colon-Rosario, V., Carver, F., Holroyd, T., DiazGranados, N., Machado-Vieira, R., Grillon, C., et al. (2010). Anterior cingulate desynchronization and functional connectivity with the amygdala during a working memory task predict rapid antidepressant response to ketamine. Neuropsychopharmacology *35*, 1415–1422.

Sheline, Y.I., Price, J.L., Yan, Z., and Mintun, M.A. (2010). Resting-state functional MRI in depression unmasks increased connectivity between networks via the dorsal nexus. Proc. Natl. Acad. Sci. USA *107*, 11020–11025.

Siapas, A.G., Lubenov, E.V., and Wilson, M.A. (2005). Prefrontal phase locking to hippocampal theta oscillations. Neuron *46*, 141–151.

Sigurdsson, T., Stark, K.L., Karayiorgou, M., Gogos, J.A., and Gordon, J.A. (2010). Impaired hippocampal-prefrontal synchrony in a genetic mouse model of schizophrenia. Nature *464*, 763–767.

Stuber, G.D., Sparta, D.R., Stamatakis, A.M., van Leeuwen, W.A., Hardjoprajitno, J.E., Cho, S., Tye, K.M., Kempadoo, K.A., Zhang, F., Deisseroth, K., and Bonci, A. (2011). Excitatory transmission from the amygdala to nucleus accumbens facilitates reward seeking. Nature *475*, 377–380.

Tennant, C. (2002). Life events, stress and depression: a review of recent findings. Aust. N. Z. J. Psychiatry *36*, 173–182.

Vialou, V., Bagot, R.C., Cahill, M.E., Ferguson, D., Robison, A.J., Dietz, D.M., Fallon, B., Mazei-Robison, M., Ku, S.M., Harrigan, E., et al. (2014). Prefrontal cortical circuit for depression- and anxiety-related behaviors mediated by cholecystokinin: role of ΔFosB. J. Neurosci. *34*, 3878–3887.

Warren, B.L., Vialou, V.F., Iñiguez, S.D., Alcantara, L.F., Wright, K.N., Feng, J., Kennedy, P.J., Laplant, Q., Shen, L., Nestler, E.J., and Bolaños-Guzmán, C.A. (2013). Neurobiological sequelae of witnessing stressful events in adult mice. Biol. Psychiatry *73*, 7–14.

Yuen, E.Y., Wei, J., Liu, W., Zhong, P., Li, X., and Yan, Z. (2012). Repeated stress causes cognitive impairment by suppressing glutamate receptor expression and function in prefrontal cortex. Neuron *73*, 962–977.

Zou, H., and Hastie, T. (2005). Regularization and variable selection via the elastic net. J. R. Stat. Soc., B *67*, 301–320.

Neuron, Volume *91*

## Supplemental Information

# Dysregulation of Prefrontal Cortex-Mediated Slow-Evolving Limbic Dynamics Drives Stress-Induced Emotional Pathology

**Rainbo Hultman, Stephen D. Mague, Qiang Li, Brittany M. Katz, Nadine Michel, Lizhen Lin, Joyce Wang, Lisa K. David, Cameron Blount, Rithi Chandy, David Carlson, Kyle Ulrich, Lawrence Carin, David Dunson, Sunil Kumar, Karl Deisseroth, Scott D. Moore, and Kafui Dzirasa**

## Supplementary Figures

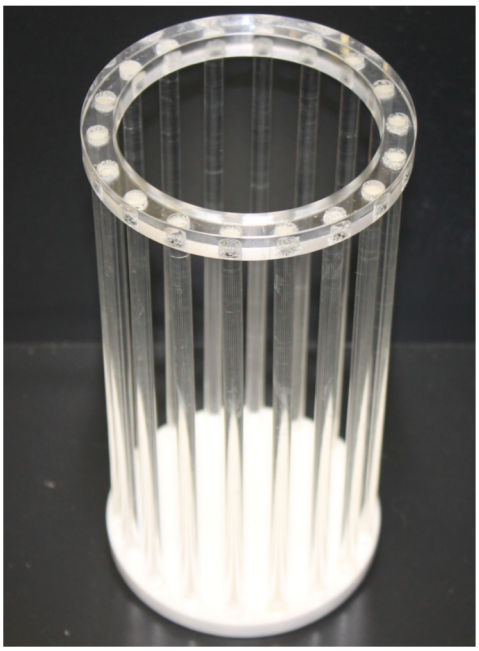

**Supplemental Figure S1:** *Related to Figure 1.* Chamber used for forced interaction test

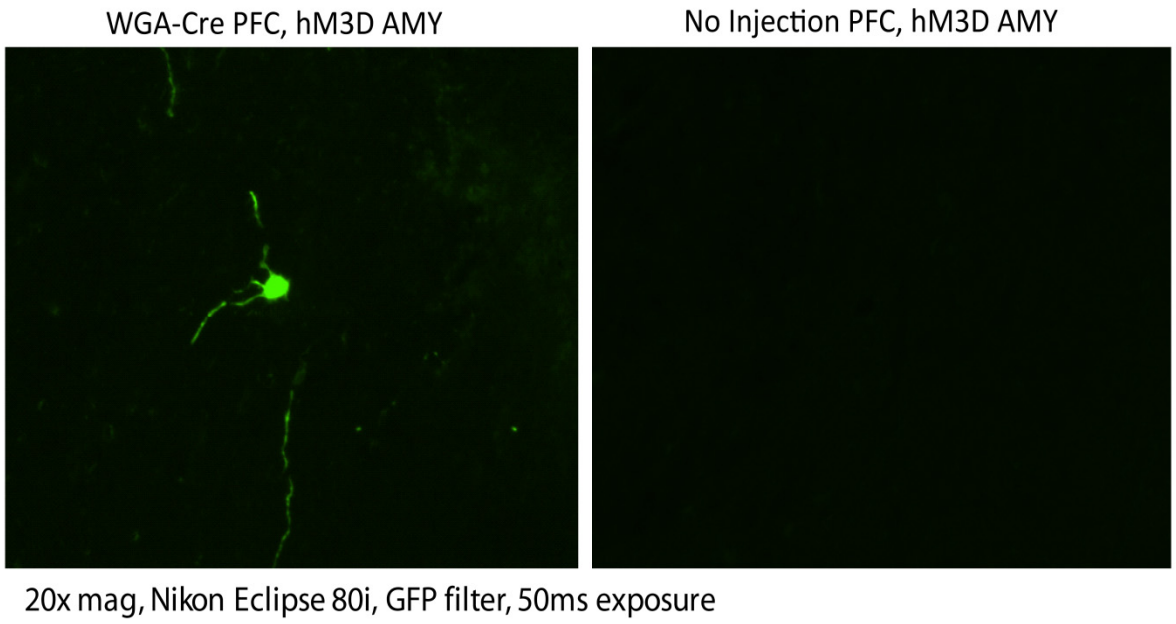


**Supplemental Figure S2:** *Related to Figure 5.* No hM3D expression was observed in the absence of WGA-Cre injection. Data are representative from four animals.

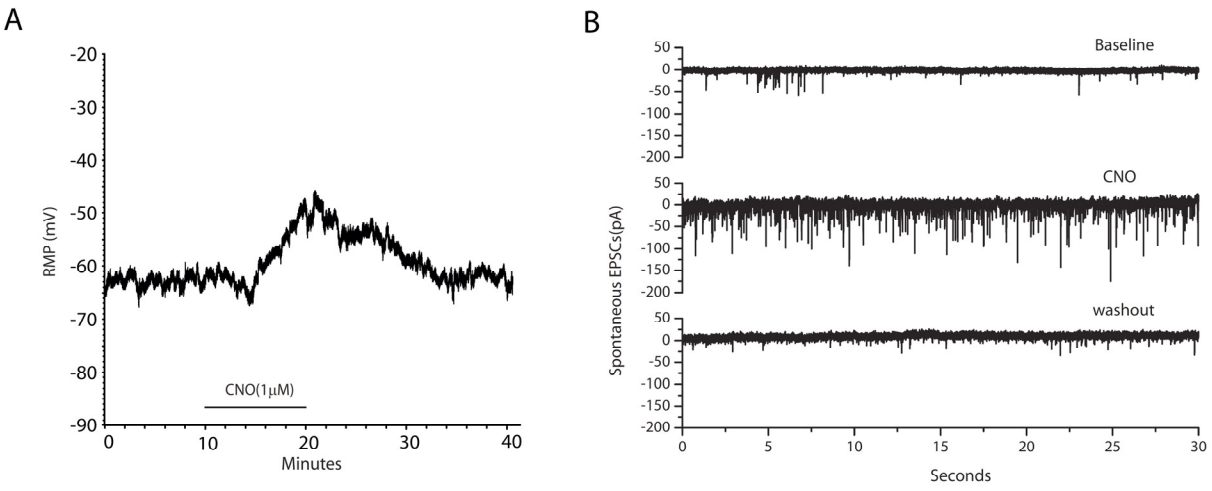


**Supplemental Figure S3:** *Related to Figure 5.* **DREADD stimulation activates AMY neurons. A)** Activation of Gq-DREADD by CNO reversibly depolarizes an AMY principal neuron. Under current clamp condition and in the presence of tetrodotoxin (1uM), picrotoxin (75uM), AP-5 (50uM) and DNQX (20uM), bath application of CNO (1uM) for 10 minutes depolarizes cell membrane potential. **B)** Activation of Gq-DREADD by CNO reversibly enhances spontaneous AMPA-EPSCs in an AMY principal neuron. The representative traces recorded during baseline (upper), bath application of CNO (1uM) (middle) and washout (bottom) are shown to demonstrate that CNO (1uM) increases spontaneous EPSCs robustly in this neuron.

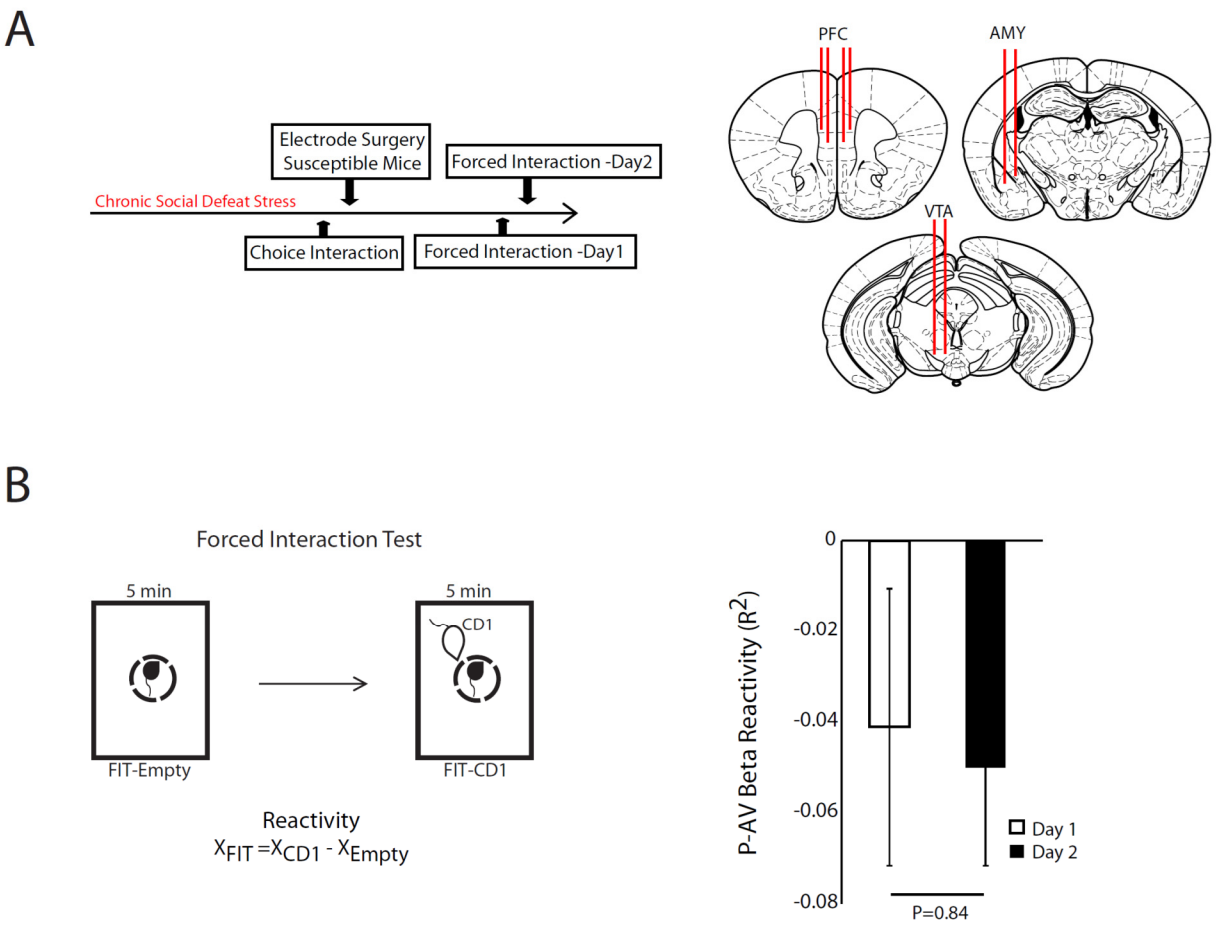


**Supplemental Figure S4:** *Related to Figure 6.* **P-AV reactivity is stable in stress susceptible mice. A)** Schematic of experimental timeline (left) and electrode implantation sites (right). **B)** The correlation between PFC activity and AMY-VTA coherence (P-AV network) was quantified during each segment of the forced interaction test (FIT; left). No differences in P-AV reactivity were observed across testing sessions. (P=1 using sign rank test; N=5 mice, right).

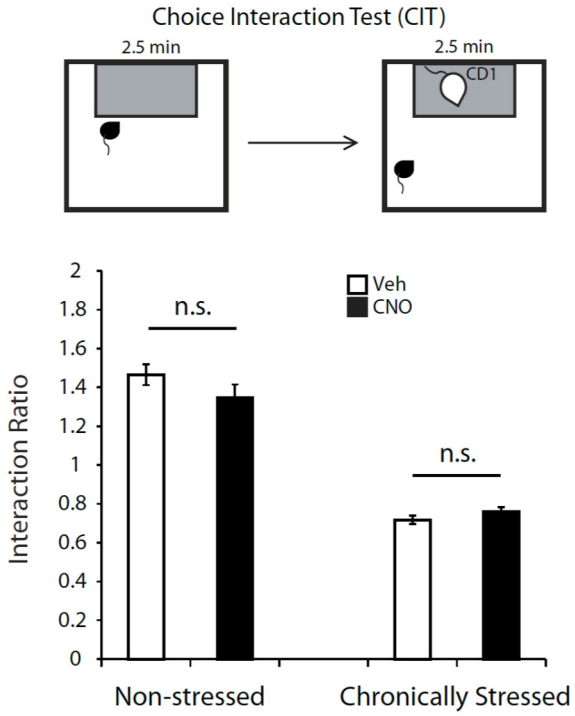


**Supplemental Figure S5:** *Related to Figure 7.* **No non-specific effects of CNO on social interaction.** Single chamber interaction ratios measured in chronically stress mice and non-stress controls. These animals were not infected with virus. Two-way ANOVA of stress by CNO treatment with a Box-Cox transform found a significant effect of stress exposure ($F_{1,69} = 20.6$, $p < 0.0001$ for stress exposure effect; N = 10 for both non-stressed groups and 24-26 for both stressed groups) but not drug on the interaction ratio ($F_{1,49} = 0.1$, $p = 0.75$ for drug effect). Additionally, there was no stress exposure x drug effect ($F_{1,69} = 0.44$, $p = 0.51$). No differences in the distribution of social interaction ratios were observed between vehicle (Veh) and CNO treated chronically-stressed mice ($p = 0.99$ using Kolmogorov-Smirnov test).

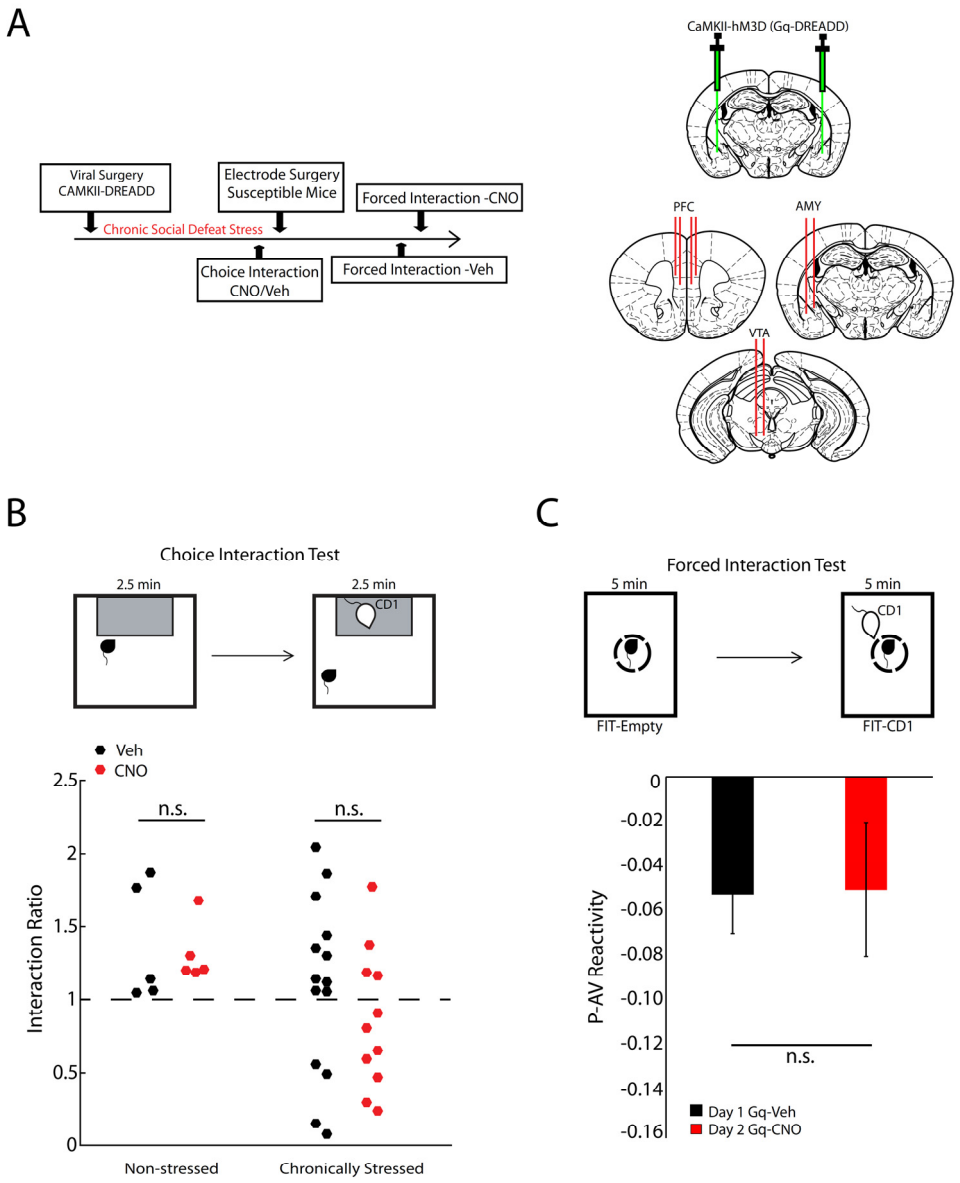


**Supplemental Figure S6:** *Related to Figure 6 and 7.* **Global AMY stimulation fails to reverse susceptible-behavior and network physiology. A)** Schematic of experimental timeline (left) and electrode implantation sites (right). **B)** Single chamber interaction ratios measured in chronically stress mice and non-stress controls infected with CaMKII-Gq-DREADD in AMY. Two-way ANOVA of stress x drug treatment with a Box-Cox transform failed to find a significant effect of drug treatment ($F_{1,34}$ = 0. 68, p = 0.42 for CNO effect; N = 5 for both non-stressed groups and 11-14 for both stressed groups) or a stress exposure x drug effect ($F_{1,34}$ = 0.22, p = 0.64). CNO-treated stressed-mice exhibited interaction ratios that were lower than the pooled group of non-stressed mice (no differences were observed in the social interaction ratios of vehicle and CNO treated chronically-stressed mice; p = 0.65 using rank-sum test), demonstrating that in contrast to PFC-AMY stimulation, global AMY stimulation did not reverse the susceptible phenotype (compare to Figure 7C in main text). **C)** Treatment with CNO had no effect on P-AV reactivity in susceptible mice (p = 0.81 using sign-rank test; N=7 mice). Viral expression was confirmed histologically in animals treated with CNO.

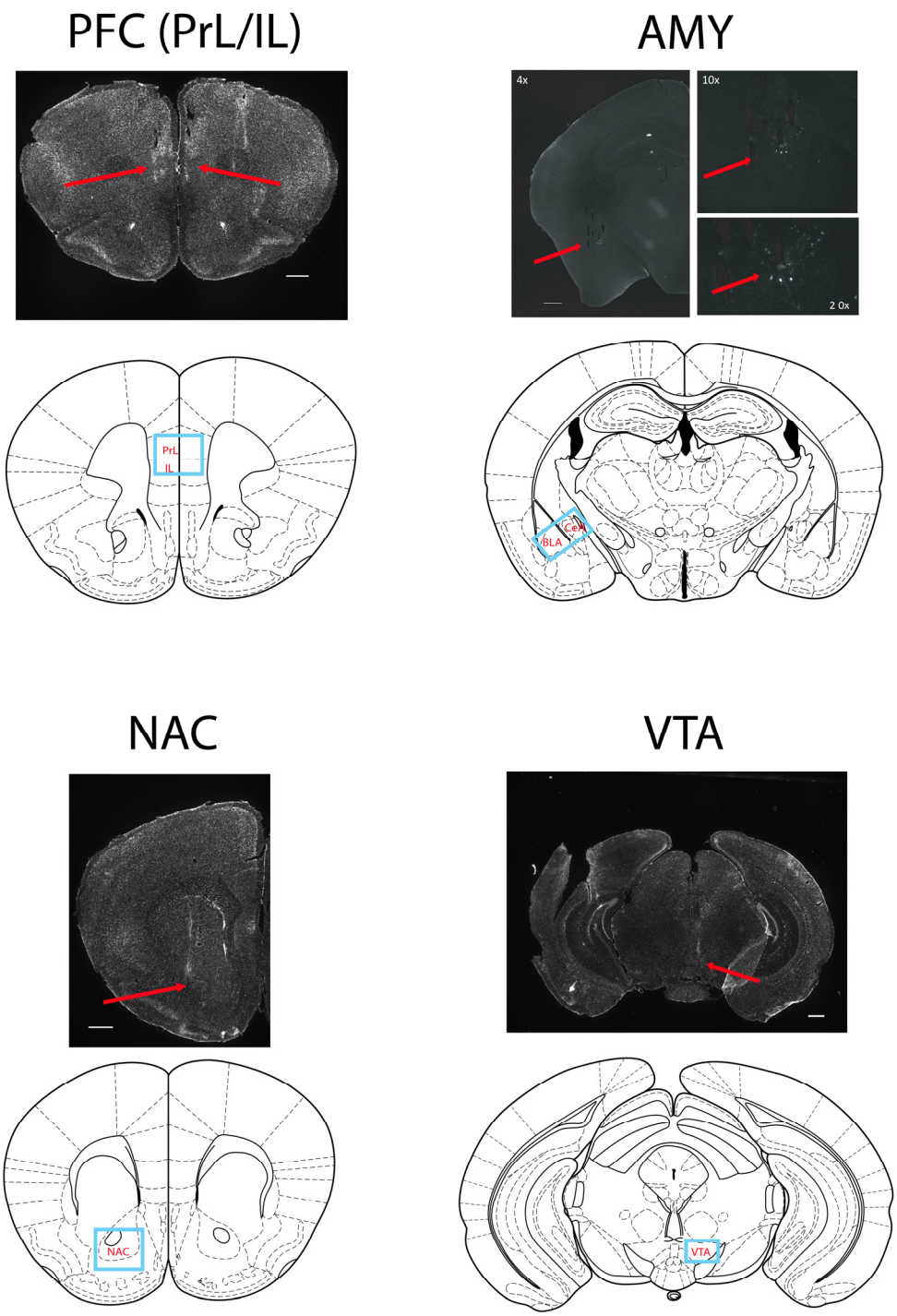


**Supplemental Figure S7:** *Related to Figure 1-3.* **Microwire implantation sites.** Co-localization of electrode tracks and DREADDs are shown in the AMY histology. Bundle tips were distributed within the blue boxes across animals. White scale bars correspond to 500µm.

## Extended Experimental Procedures Materials

**Animal Care and Use**

C57BL/6J (C57) male mice purchased from the Jackson Labs and CD1 male mice purchased from Charles River Laboratory were used for all experiments presented in this study. Mice were housed on a 12 hour light/dark cycle, and maintained in a humidity- and temperature-controlled room with water and food available *ad libitum*. C57 mice were initially housed three-five/cage and separated after surgery. All CD1 mice were single-housed. Studies were conducted with approved protocols from the Duke University Institutional Animal Care and Use Committee and were in accordance with the NIH guidelines for the Care and Use of Laboratory Animals.

**Single chamber social interaction test**

For DREADDs experiments, animals were injected (intraperitoneally with either CNO (1mg/kg; Enzo Life Sciences, Farmingdale, NY) or vehicle (20% Captisol, Cydex Pharmaceuticals, Lawrence KS) 45 minutes prior to the test. Mice were placed within a novel arena (46cm x 46cm) with a small cage located at one end, and each mouse's movement was monitored for 150 seconds. Mice were then removed from the testing chamber, and reintroduced 30 seconds later after a non-aggressive CD1 mouse was placed in the small cage. Locomotor activity measurements (distance traveled) and time spent in the interaction zone were quantified using Ethovision XT 7.1 software (Noldus Information Technology, Wageningen, Netherlands). The interaction ratio was calculated as (interaction time, CD1 present)/(interaction time, CD1 absent) (Golden et al., 2011; Kumar et al., 2014).

**Electrode Implantation Surgery**

The recording bundles designed to target AMY, NAc, VTA, and PFC were centered based on stereotaxic coordinates measured from bregma (AMY: -1.6mm AP, 2.75 mm ML, -3.9 mm DV from the dura; NAc: 1.6mm AP, 1.4mm ML, -3.5 mm DV from the dura; PFC: 1.7mm AP, 0mm ML, 2.25mm DV from the dura; VTA: -3.3mm AP, 0.5 mm ML, -4.25 mm DV from the dura). Several animals were implanted in

ventral subiculum as well (vSub: -3.7mm AP, 3.0mm ML, -3.5mm DV from the dura); however, neural data recorded from this brain region was not used in this study. Implanted electrodes were anchored to ground screws using dental acrylic. Experiments were initiated following a two week recovery. The full details of our electrode construction and surgical implantation procedures have been previously described (Dzirasa et al., 2011).

**Chronic social defeat stress**

Mice implanted with electrodes underwent 10 days of chronic social defeat stress as previously described (Berton et al., 2006; Covington et al., 2010). Male, retired-breeder CD1 (Charles River) mice were used as resident aggressors for the social defeat and were singly-housed prior to the experiments. Particularly aggressive CD1s, as defined by demonstrating at least one successful act of aggression toward an intruder C57 male within 60 sec, were selected for use during the social defeat. Mice were singly housed prior to undergoing social defeat. Intruder male C57 mice were introduced to the cage of a novel CD1 aggressor for 5 min daily, and then housed adjacent to the same aggressor for 24 hours. During this time, mice were separated by a transparent and porous plexiglass barrier to enable constant sensory exposure. During bouts of exposure to the CD1 mice, hallmark behavioral signs of subordination stress were observed including escape, submissive postures (i.e., defensive upright and supine), and freezing. Following the last 24 hr exposure to a CD1 aggressor mouse, all C57s were housed individually. Mice that exhibited significant injuries during social defeat stress were removed from further analysis.

**Forced Interaction test (FIT)**

C57 mice were placed in a 3.25" x 7" Plexiglas cylinder (Noldus, see Supplemental Fig. S1). Following a five minute recording period during which neurophysiological activity was recorded, a CD1 aggressor mouse was introduced to the cage outside of the cylinder (18" high walls surround the outer cage to prevent escape and a lid is place over the inner chamber to prevent the aggressor from climbing in). Neurophysiological data were then recorded for an additional five minutes. All animals were subjected

to the FIT after exposure to chronic social defeat stress. Additionally, all of the mice implanted with electrodes prior to social defeat were subjected to a pre-stress FIT (these data were not included in this study).

**Three-chamber social interaction test**

The social interaction chamber consisted of a 25”x 16”arena separated into 3 equivalent chambers by partial dividers. Mice were able to move between the chambers through a space in the center of each divider. Each of the two end chambers contained a cylindrical sub-chamber. One sub-chamber contained a CD1 mouse, and the other sub-chamber was empty. Social interaction was quantified in mice following exposure to chronic subordination stress. C57 mice were placed in the center chamber and video recordings were acquired as mice explored the three-chamber apparatus for five minutes. The duration of time mice spent in each chamber as well as in a smaller proximal interaction zone directly adjacent to the social target was quantified using Ethovision XT 7.1 (Noldus Information Technology, Wageningen, Netherlands) software.

**LFP directionality analysis**

LFP data acquired from the second segment of the FIT (during exposure to the CD1) was filtered using butterworth bandpass filters designed to isolate LFP oscillations within a 2Hz window using a 1Hz step (1-55Hz). The instantaneous phase of the filtered LFPs were then determined using the Hilbert transform, and the instantaneous phase offset time series was calculated for each LFP pair $(\phi_{Area2} - \phi_{Area1})_t$. The mean resultant length (MRL) for the phase offset time series, corresponding to the deviation from circular uniformity (where 0 represents no deviation from circular uniformity and 1 represents a perfect distribution at a single angle/phase) then represents the phase coherence between the pair of LFPs. We then introduced temporal offsets between the two LFPs ranging from [-250ms to 250ms] in 1 ms steps and recalculated the phase coherence between the LFP pair. The offset at which the two LFPs optimally phase synchronized established the directionality. To confirm that PFC and AMY exhibited directionality

in the beta frequency range (14-23Hz), we calculated LFP phase coherence at various temporal offsets in a second group of animals implanted with wires in PFC and AMY. These mice were previously recorded as part of a prior study (Kumar et al., 2014), though data were not analyzed in the 15-30Hz range.

**Determination of LFP oscillatory power and cross-area synchrony**

Signals recorded from all of the implanted microwires were used for analysis. Using Matlab (The MathWorks, Inc., Natick, MA), a sliding Fourier transform with Hamming window was applied to the LFP signal using a 1 second window and a 1 second step. Frequencies were analyzed with a resolution of 1Hz. LFP oscillatory power was averaged across all LFP channels for a given brain area. LFP cross-structural coherence was calculated from LFP pairs using magnitude-squared coherence

$$C_{AB}(f) = \frac{|Psd_{AB}(f)|^2}{Psd_{AA}(f)Psd_{BB}(f)}$$

where coherence is a function of the power spectral densities of A and B, and their cross-spectral densities. These calculated coherence values were then averaged across all wires recorded from a given brain area pair. LFP activity was averaged within frequency bands of interest, and the correlation between LFP measures was calculated using a spearman rank regression for each segment of the FIT. Periods of LFP saturation (1.8±0.5% of the data/mouse; N = 55 recording sessions) were excluded from this analysis.

**Single unit phase locking and phase-offset locking**

AMY and VTA LFPs were filtered using Butterworth bandpass filters designed to isolate LFP oscillations within the beta (14–23Hz) frequency range. The instantaneous phase of the filtered LFP was then determined using the Hilbert transform, and phase locking was detected using the Rayleigh test at $\alpha$=0.05 (Jacobs et al., 2007; Siapas et al., 2005). Phase-offset locking was measured based on the mean resultant length (MRL) of neuronal firing relative to the instantaneous phase offset between AMY and VTA beta oscillations. Neurons which exhibited MRL values outside of the 95% confidence interval expected for the chance distribution were deemed to show significant phase-offset locking.

**Viral Histology**

At the completion of all behavioral and neurophysiological studies, mice were perfused transcardially with 4% PFA (EM Sciences, Hatfield, PA) and brains were harvested, frozen, and sliced at 35µm using a cryostat (Cryocut 1800, Reichert-Jung, Depew, NY) and stained with an anti-GFP antibody at a dilution of 1:2000 (rabbit polyclonal, A11122, Invitrogen, Grand Island, NY) overnight at 4C after 1hr in blocking buffer (3% goat serum, Gibco, Grand Island, NY ;0.25% Triton X-100, Amresco, Solon, OH) to confirm expression of viral vector in the AMY. Following three two-hour washes in blocking buffer at 4C, an Alexa-Fluor-488 goat anti-rabbit secondary antibody (A11008, Invitrogen, Grand Island, NY) was used at 1:2000 overnight at 4C followed by two washes in blocking buffer and a final wash in PBS. A mild acetate buffer was used for mounting brains on slides (82.4mM Sodium Acetate, 17.6mM acetic acid).

**Measuring effect of PFC-AMY circuit activation on stress induced behavioral dysfunction**

For behavior experiments, data from four cohorts were pooled, and mice were separated into susceptible and unsusceptible groups based on their proximal interaction scores in the three-chamber test. Briefly, previous studies have demonstrated that high proximal interaction times during social interaction tests are sufficient to identify stress-unsusceptible mice (Covington et al., 2010; Krishnan et al., 2007). Thus, we pooled all of the three chamber social interaction measured in stressed mice (prior to confirmation of viral expression in the mice). These data were then used to determine the upper $40^{th}$ percentile of interaction scores, and mice that exhibited total interaction scores above this threshold were analyzed separately. This approach was used to exclude mice that were likely to be stress-unsusceptible (i.e. resilient) from the subsequent single chamber DREADD analysis in susceptible animals.

After excluding the 'likely unsusceptible/resilient' population, we evaluated animals by group based on their viral treatment (GFP versus Gq-DREADD). Comparisons were made between the interaction ratios observed in Gq-DREADD and GFP-control (non-stressed) groups during the single chamber social interaction test (CNO treated) using a two-way ANOVA with a Box-Cox transform applied to the interaction ratio scores. Direct comparisons were then made within condition (Gq-DREADD vs. GFP-Control) using a

rank-sum test. Only GFP infected mice, and Gq-DREADD infected mice with receptor expression confined to AMY (confirmed by histology) were included in the single chamber social interaction test data analysis (N=27/53 total mice infected with Gq-DREADD).

**Evoked AMPA receptor-mediated excitatory postsynaptic currents (EPSCs)**

Evoked AMPA receptor-mediated EPSCs were isolated by bath application of picrotoxin (75μM), AP-5 (50μM) and CGP55845 (1μM) to block $GABA_A$ receptor-mediated inhibitory transmission, NMDA receptor-mediated excitatory transmission and presynaptic $GABA_B$ autoreceptors, respectively. A monopolar stimulating electrode was placed approximately 50 μm away from the patched neurons and evoked responses were recorded from AMY principal neurons held at -70 mV at a stimulus frequency of 0.1 Hz (stimulus duration 0.01-0.02 msec). After the input-output curve was determined, the stimulus intensity was adjusted to evoke a response at 50% of the maximum.

**Evoked $GABA_A$ receptor-mediated inhibitory postsynaptic currents (IPSCs)**

In a separate series of experiments, evoked IPSCs were isolated in the presence of either kynurenic acid (3mM) or AP-5 (50μM) and DNQX (20μM) to block glutamatergic transmission and CGP55845 (1.0μM). The stimulation protocol was otherwise the same as that used for EPSCs as described above.

## Detailed Author Contributions

RH designed experiments; performed *in vivo* electrophysiological, viral, and behavioral experiments; histology, analyzed *in vivo* electrophysiological and behavioral data; and wrote the paper with KDz, QL, SDM.
SMa performed *in vivo* electrophysiology and viral experiments, histology; and helped write the paper.
QL conceived, performed, and analyzed *in vitro* electrophysiology experiments; and wrote the paper
BK performed *in vivo* electrophysiology, viral, and behavioral experiments; and performed histological analysis of implantation sites.
NM performed *in vivo* electrophysiology, viral, and behavioral experiments; and performed histological analysis of implantation sites.
LL assisted with analysis of behavioral and neurophysiological data.
JW assisted with electrode implantation surgeries and behavioral experiments; and performed histological analysis of implantation sites
LD assisted with behavioral experiments, and histological analysis of implantation sites
CB performed histological analysis of implantation sites
RC assisted with behavioral experiments, and histological analysis of implantation sites
DC conceived network analysis approaches with KU
KU conceived network analysis approaches with DC
LC oversaw statistical analyses with DD and KDz; and helped to write the paper
DD oversaw statistical analyses with LC and KDz; and helped to write the paper
SK performed *in vivo* electrophysiology experiments.
KDe helped to conceive optogenetic experiments and provided viral tools
SDM conceived in vitro electrophysiology experiments, and wrote the paper with
SMa, RH, KDz, QL.
KDz conceived electrophysiological, viral and behavioral experiments; analyzed *in vivo* electrophysiological and behavioral data with RH, and wrote the paper with RH, SMa, QL, SDM.

## Supplementary References


Berton, O., McClung, C.A., Dileone, R.J., Krishnan, V., Renthal, W., Russo, S.J., Graham, D., Tsankova, N.M., Bolanos, C.A., Rios, M.*, et al.* (2006). Essential role of BDNF in the mesolimbic dopamine pathway in social defeat stress. Science 311, 864-868.

Covington, H.E., 3rd, Lobo, M.K., Maze, I., Vialou, V., Hyman, J.M., Zaman, S., LaPlant, Q., Mouzon, E., Ghose, S., Tamminga, C.A.*, et al.* (2010). Antidepressant effect of optogenetic stimulation of the medial prefrontal cortex. J Neurosci 30, 16082-16090.

Dzirasa, K., Fuentes, R., Kumar, S., Potes, J.M., and Nicolelis, M.A. (2011). Chronic in vivo multi-circuit neurophysiological recordings in mice. Journal of neuroscience methods 195, 36-46.

Golden, S.A., Covington, H.E., 3rd, Berton, O., and Russo, S.J. (2011). A standardized protocol for repeated social defeat stress in mice. Nature protocols 6, 1183-1191.

Jacobs, J., Kahana, M.J., Ekstrom, A.D., and Fried, I. (2007). Brain oscillations control timing of single-neuron activity in humans. J Neurosci 27, 3839-3844.

Krishnan, V., Han, M.H., Graham, D.L., Berton, O., Renthal, W., Russo, S.J., Laplant, Q., Graham, A., Lutter, M., Lagace, D.C.*, et al.* (2007). Molecular adaptations underlying susceptibility and resistance to social defeat in brain reward regions. Cell 131, 391-404.

Kumar, S., Hultman, R., Hughes, D., Michel, N., Katz, B.M., and Dzirasa, K. (2014). Prefrontal cortex reactivity underlies trait vulnerability to chronic social defeat stress. Nat Commun 5, 4537.

Siapas, A.G., Lubenov, E.V., and Wilson, M.A. (2005). Prefrontal phase locking to hippocampal theta oscillations. Neuron 46, 141-151.